

# An Antagomir to MicroRNA-106b-5p Ameliorates Cerebral Ischemia and Reperfusion Injury in Rats Via Inhibiting Apoptosis and Oxidative Stress

Pengfei Li<sup>1</sup> · Meihong Shen<sup>2</sup> · Feng Gao<sup>1</sup> · Jinping Wu<sup>3</sup> · Jiahui Zhang<sup>3</sup> · Fengmeng Teng<sup>1</sup> · Chunbing Zhang<sup>1,3</sup>

Received: 3 December 2015 / Accepted: 9 March 2016 / Published online: 29 March 2016  
© Springer Science+Business Media New York 2016

**Abstract** We previously observed that microRNA miR-106b-5p significantly increased in serum of patients with acute ischemic stroke. The present study was to determine whether miR-106b-5p antagomir can protect against cerebral ischemia/reperfusion (I/R) injury and elucidate its underlying mechanisms. Middle cerebral artery occlusion (MCAO) was operated on male Sprague Dawley rats. MiR-106b-5p antagomir significantly decreased neurological deficit scores, infarct volumes, and neuronal injury. Furthermore, miR-106b-5p antagomir markedly reduced malondialdehyde (MDA) content, restored superoxide dismutase (SOD) activity, increased the expression of myeloid cell leukemia-1 (Mcl-1) and B cell lymphoma-2 (Bcl-2), and decreased the expression of Bax in the ischemic cortex. In PC12 cells, miR-106b-5p inhibitor increased the Mcl-1 and Bcl-2 expression, which provided protection against glutamate-induced apoptosis and oxidative damage, as evidenced by decreased lactate dehydrogenase (LDH) release, and enhanced SOD activity. Notably, luciferase reported assay proved Mcl-1 was the target gene of miR-106b-5p. In conclusion, our data indicates that the neuroprotective effects of miR-106b-5p antagomir on cerebral I/R

injury are associated with its inhibition of apoptosis and oxidative stress, suggesting a potential therapeutic target for ischemic stroke.

**Keywords** MiR-106b-5p · Ischemic stroke · Middle cerebral artery occlusion · Apoptosis · Oxidative stress

## Abbreviations

MiRNA	MicroRNA
MCAO	Middle cerebral artery occlusion
CNS	Central nerve system
IS	Ischemic stroke
I/R	Ischemia/reperfusion
MDA	Malondialdehyde
Bcl-2	B cell lymphoma-2
LDH	Lactate dehydrogenase
SOD	Superoxide dismutase
ROS	Reactive oxygen species
TTC	2,3,5-Triphenyltetrazolium chloride
HE	Hematoxylin and eosin
MRI	Magnetic resonance imaging
FITC	Fluorescein isothiocyanate
ROS	Reactive oxygen species
3'-UTR	3'-Untranslated region
MCM7	Mini chromosome maintenance protein 7
SEM	Standard error of the mean
PI	Propidium iodide

Pengfei Li and Meihong Shen contributed equally to this work.

✉ Chunbing Zhang  
zzzcb99@163.com

<sup>1</sup> Department of Clinical Laboratory, Jiangsu Province Hospital of Traditional Chinese Medicine, Affiliated Hospital of Nanjing University of Chinese Medicine, Nanjing 210029, Jiangsu, China

<sup>2</sup> The Second Clinical College, Nanjing University of Chinese Medicine, Nanjing 210046, Jiangsu, China

<sup>3</sup> Basic Medical Sciences, Nanjing University of Chinese Medicine, Nanjing 210046, Jiangsu, China

## Introduction

Stroke, a serious damage to public health, has high incidence, high morbidity, and high mortality characteristics. It can be classified into ischemic stroke (IS) and hemorrhagic stroke

(HS). IS accounts for approximately 87 % of all stroke cases [1]. Although the exact molecular mechanisms of stroke-induced neurological dysfunction are not fully known, the important roles of apoptosis and oxidative stress after stroke have emerged as an attractive field [2]. Hence, anti-apoptotic or anti-oxidative agents might benefit the treatment of cerebral ischemia damage.

MicroRNAs (miRNAs) are small non-coding endogenous RNAs (~22 nt) that negatively modulate gene expression by binding to the 3'-untranslated region (3'-UTR) of target messenger RNA (mRNA) [3]. MiRNAs are highly conserved and are able to regulate a wide range of biological processes including cell proliferation and differentiation, metabolism, and apoptosis [4]. Especially, miRNAs are expressed abundantly in the central nerve system (CNS) and have critical roles in normal CNS development and function [5, 6], as well as in cerebral diseases including stroke [7]. Motivated by this, extensive reports have demonstrated differential miRNA expression in animal models [8] and stroke patients [9]. We had also previously performed the global profile of miRNAs in acute IS patients using miRNA microarray and found that several miRNAs, including miR-106b-5p, significantly increased [10].

MiR-106b-5p, the member of miR-106b~25 clusters (miR-106b, miR-93, and miR-25), is located on human chromosome 7q21. MiR-106b-5p has been reported to be aberrantly expressed in various cancers in humans [11–13]. Interestingly, circulating miR-106-5p has been proposed as a novel biomarker for epilepsy [14], gastric cancer [15], and B cell lymphoma [16]. Up to now, several articles have confirmed the neuroprotective effects of miRNAs against middle cerebral artery occlusion (MCAO) models [17–19]. Furthermore, a few of miRNAs have evidence to support their anti-ischemic or anti-oxidative properties [20–22]. The roles of miR-106b-5p in IS, however, remain largely elusive. In the present study, we performed a comprehensive investigation *in vitro* and *in vivo*, exploring the underlying molecular mechanisms of miR-106b-5p on stroke.

## Materials and Methods

### Animals and Experimental Groups

Adult male Sprague Dawley rats (SD, 250–280 g) were provided by Vital River Laboratory Animal Technology Co. Ltd (Beijing, China). The rats were housed in the same temperature- and humidity-controlled animal facility with a 12-h light/dark cycle. A total of 72 adult male SD rats were randomly separated into 4 groups: (1) sham group ( $n=18$ ), (2) MCAO group ( $n=18$ ), (3) miR-106b-5p antagomir group ( $n=18$ ), and (4) antagomir control group ( $n=18$ ).

### Middle Cerebral Artery Occlusion/Reperfusion Model

According to a previous description [23], the rats were subjected to MCAO and reperfusion operations. Briefly, the rats were initially anesthetized with 10 % chloral hydrate (Abbott, IL, USA). A 4-0 monofilament nylon suture (Ethicon Johnson & Johnson, Brussels, Belgium) with a heat-blunted end was inserted into the right external carotid artery and advanced into the internal carotid artery until it occluded the origin of the middle cerebral artery. After 2 h of MCAO, the rats were reperfused by removing the suture from the vessel. Rectal temperature was maintained around 37 °C throughout the surgical procedure using a heating lamp and the thermo-controlled base of the operating table. In the sham-operated groups, the external carotid artery was surgically prepared for insertion of the filament but the filament was not inserted.

### Drug Administration

In the miR-106b-5p antagomir and antagomir control groups, the rats went through the MCAO surgical procedures. The MiR-106b-5p antagomir (50 nmol/kg) or antagomir control (50 nmol/kg) was administrated by tail venous injection at the beginning of reperfusion. The MiR-106b-5p antagomir and antagomir control were obtained from GenePharma (Shanghai, China) and dissolved in DEPC-treated H<sub>2</sub>O.

### Neurological Scoring

The animals subjected to MCAO underwent neurological function evaluation at 24 h after MCAO surgical procedure. Neurological assessment was performed using a modified 6-point scoring system [24]: score 0, normal motor function; score 1, flexion of the torso and contralateral forelimb when the rat was lifted by the tail; score 2, circling when the rat was held by the tail on a flat surface; score 3, leaning to one side at rest; score 4, no spontaneous motor activity; and score 5, death within 24 h. A single observer blinded to group assignment performed neurological testing.

### 2,3,5-Triphenyltetrazolium Chloride Staining

2,3,5-Triphenyltetrazolium chloride (TTC; Sigma, St. Louis, MO, USA) staining was used for detecting infarction volume. In brief, at 24 h after reperfusion, the rats ( $n=6$ ) were decapitated, and the brains were rapidly removed and sectioned into five coronal blocks with an approximate thickness of 2 mm. The sections were stained with 2 % TTC for 30 min at 37 °C in the dark followed by overnight immersion in 4 % paraformaldehyde. The infarcted tissue remained unstained (white), whereas normal brain tissues were stained red. The infarct zone was measured using ImageJ (NIH, USA). The total

infarction volume was calculated by integrating five sections, manually measuring the infarct as previously described [25].

### Magnetic Resonance Imaging

MRI measurements were obtained 24 h after MCAO. The rat brains were further tested in a 7.0-T MRI animal scanner (Magnetom Trio with TIM system, Siemens, Erlangen, Germany). In order to detect the signal excitation, the rat's head was placed in a custom-made "birdcage coil," with a 30-mm inner diameter. Magnetic resonance imaging (MRI) parameters were set as follows: TE=40 ms, TR=3000 ms, FOV=3.5 cm,  $M=256 \times 256$ , thickness=1 mm, and gap=1 mm. Images acquired with T2-weighted sequences were used to generate T2 maps that were further analyzed using ImageJ. Irregular regions of interest (ROIs) were drawn to encircle the entire stroke lesion exhibited as a hyperintensity area in each T2 map. The delineated lesion areas were summed and multiplied by the slice thickness to determine the infarct volume.

### Histopathological Examination

Hematoxylin and eosin (HE) staining was performed to show the morphological features of injured neurons in the cerebral cortex. At 24 h after reperfusion, the rats were sacrificed and the brains were fixed by transcardial perfusion with PBS, followed by perfusion and immersion in 4 % paraformaldehyde. The brains were then dehydrated in a graded series of alcohols and embedded in paraffin. A series of 6- $\mu$ m-thick sections were cut from the block. Finally, the sections were stained with HE reagents for pathological histological examination.

### Immunohistochemistry Analysis

At 24 h after reperfusion, the rats were deeply anesthetized with chloral hydrate and perfused with PBS, followed by perfusion with 4 % paraformaldehyde. The brain tissue samples were cut into three blocks and were embedded in paraffin. The paraffin-embedded tissues were sectioned at 6  $\mu$ m. After deparaffinization, the sections were boiled in 0.2 % citrate buffer for 15 min and immersed in PBS containing 0.3 % Triton X-100 and 10 % normal goat serum for 1 h at room temperature (RT). After incubation with rabbit anti-Bax (1:150; Abcam, Cambridge, UK) monoclonal antibodies and rabbit anti-Bcl-2 (1:200, Santa Cruz Biotechnology, Santa Cruz, CA) polyclonal antibodies in 0.01 mol/L PBS overnight at 4 °C, the sections were washed with PBS and incubated with horseradish peroxidase-labeled secondary antibodies for 1.5 h at RT. The specific staining was visualized using a diaminobenzidine (DAB) kit (Boster, Wuhan, China). A light

microscope, Leica DM4000 (Leica, Germany), was used to obtain images at  $\times 400$  magnification. The morphometric examination was performed in a blinded manner by two independent investigators. For each section, five visual fields were chosen at random for statistical analysis. Results were expressed as the mean optical density of the Bax or Bcl-2 immunopositive cells ( $n=6$  in each group).

### PC12 Cell Culture and Treatment

The differentiated PC12 cells, a rat pheochromocytoma cell line (American Type Culture Collection, Manassas, VA, USA), were cultured in Dulbecco's modified Eagle's medium (DMEM) (Invitrogen, Carlsbad, CA) supplemented with 10 % heat-inactivated fetal bovine serum, 100 U/mL penicillin, and 100 mg/mL streptomycin (Invitrogen) in a water-saturated atmosphere of 5 % CO<sub>2</sub> at 37 °C. The medium was changed every other day. The PC12 cells were plated at an appropriate density on culture plates according to each experimental scale and cultured for 24 h. Then, the PC12 cells were treated with glutamate (Sigma) at different concentrations (12.5, 25, 50 mmol/L) and for different times (4, 8, 12, 24 h).

### Real-Time Polymerase Chain Reaction

Total RNA was isolated from the PC12 cells and rat cerebral cortex by TRIzol reagent (Invitrogen) according to the manufacturer's protocol. One microgram of RNA was subjected to reverse transcription using SuperScript III reverse transcriptase (Invitrogen). Real-time PCR for genes *Mcl-1*, *Bax*, *Bcl-2*, and *GAPDH* mRNA was performed on an Applied Biosystems 7500 Sequence Detection System (Applied Biosystems, Foster City, CA) using a universal probe library (UPL) probe (Roche, Basel, Switzerland). The primer sequences were as follows: *Bcl-2* (forward: 5'-GTACCTGAACCGGCATCTG-3', reverse: 5'-GGGGCCATATAGTTCCACAA-3', Probe name #75), *Mcl-1* (forward: 5'-CTACTGGAGCGCGTGAGC-3', reverse: 5'-GGTACAGCTCGTCGCTTCC-3', Probe name #70), *Bax* (forward: 5'-CCGAGCTGATCAGAACCATC-3', reverse: 5'-GTGGGGTCCC GAAGTAG-3', Probe name #130), and *GAPDH* (forward: 5'-CCCTCTGGAAAGCTGTGG-3', reverse: 5'-AGTGGATGCAGGGATGATG-3', Probe name #26). Mature miR-106b-5p expression was also carried out using the UPL probe as previously reported [10]; U6 snRNA was set as the internal reference control. The reactions were incubated in a 96-well optical plate at 95 °C for 10 min, followed by 40 cycles of 95 °C for 15 s and 60 °C for 1 min. The threshold cycle (Ct) value was defined as the fractional cycle number at which the fluorescence passes the fixed threshold. Relative changes in gene expression were quantified by applying the comparative Ct after determining the Ct

values for the reference gene and the target genes in each sample set according to the  $2^{-\Delta\Delta C_t}$  method. All the experiments were done in triplicate.

### MiR-106b-5p Transfection

Mimic of miR-106b-5p was a duplex RNA, with the sense sequence (5'-UAAAGUGCUGACAGUGCAGAU-3') and the antisense sequence (5'-CUGCACUGUCAGCACUUUAUU-3'). The inhibitor of miR-106b-5p (5'-AUCUGCACUGUCAGCACUUUA-3') was a single RNA sequence exactly complementary to miR-106b-5p. Non-targeting negative control sequences (for mimic: sense 5'-UUCUCCGAACGUGUCACGUTT-3', antisense 5'-ACGUGACACGUUCGGAGAATT-3'; for inhibitor: 5'-CAGUACUUUUGUGUAGUACAA-3') were used as controls. All of the above sequences were custom-synthesized by GenePharma. The transfection was performed using Lipofectamine RNAiMAX™ transfection agent (Invitrogen) in OPTI-MEMI reduced serum medium (Gibco, Grand Island, NY) according to the manufacturer's instruction. The final concentration of the miR-106b-5p mimic and mimic negative control was 50 nmol/L, and the concentration of the inhibitor of miR-106b-5p and inhibitor negative control was 100 nmol/L. The PC12 cells were harvested 48 h post-transfection for subsequent experiments.

### Apoptosis Assay

For the apoptosis assay, the PC12 cells were harvested and stained by an Annexin V-FITC apoptosis detection kit (Biouniquer Technology, Nanjing, China) according to the manufacturer's instructions. Five microliters of Annexin V-fluorescein isothiocyanate (FITC) and 5  $\mu$ L of propidium iodide (PI) were added to the cells, which were resuspended in 500  $\mu$ L of 1 $\times$  binding buffer. The cells were gently vortexed and incubated in the dark at RT for 15 min, and then analyzed using a BD FACS Canto™ II flow cytometer (BD Biosciences, San Jose, CA, USA) within 1 h. A minimum of 10,000 cells were analyzed in each treatment group. This dual staining can discriminate intact cells (AV<sup>-</sup>/PI<sup>-</sup>), early apoptotic/apoptotic cells (AV<sup>+</sup>/PI<sup>-</sup>), late apoptotic/necrotic cells (AV<sup>+</sup>/PI<sup>+</sup>), and necrotic cells (AV<sup>-</sup>/PI<sup>+</sup>). The analysis of apoptotic cells was performed using BD FACS Diva software (BD Biosciences).

### Evaluation of Cell Injury

Cell injury was assessed by morphological examination with a phase-contrast microscope, Olympus IX51 (Olympus, Japan), and by measuring the amount of lactate dehydrogenase (LDH) released into the culture medium using a diagnostic kit (Jiancheng Institute of Biotechnology, Nanjing, China)

according to the manufacturer's instructions. Briefly, 100  $\mu$ L cell culture supernatant from each well was incubated with nicotinamide-adenine dinucleotide (NADH) and pyruvate for 15 min at 37 °C. Then, the reaction was stopped with 0.4 mol/L NaOH. The activity of LDH was calculated after detection at 440 nm using a microplate spectrophotometer UV-2401 (Shimadzu Corporation, Japan). The change in absorbance was expressed in concentration units per liter.

### Assessment of Oxidative Stress

Determination of oxidative stress markers including the malondialdehyde (MDA) level and the activity of the antioxidant enzyme superoxide dismutase (SOD) in the PC12 cells and homogenates extracted from the cortex of the ischemic hemisphere of the brain was performed according to the commercial assay kits (Jiancheng Institute of Biotechnology). SOD activity was measured by the ability to inhibit the formation of formazan dye with maximum absorbance at 450 nm. The formazan dye was produced by monosodium salt reacting with O<sub>2</sub><sup>-</sup> from the xanthine oxidase system. The content of MDA was assessed at 532 nm by reacting with thiobarbituric acid to form a chromophoric product. The activity of SOD and the level of MDA in the cortex were expressed as units per milligram of protein and nanomoles per milligram protein, respectively. The activity of SOD and the level of MDA in the PC12 cell supernatant were expressed as units per milliliter and nanomoles per milliliter, respectively.

### Bioinformatics Target Gene Prediction, Gene Ontology, and Pathway Analysis

We used the miRBase (<http://www.ebi.ac.uk/enright-srv/microcosm>), TargetScan (<http://www.targetscan.org>), and miRanda (<http://www.microRNA.org>) target prediction databases for the evaluation of predicted mRNA targets. The gene ontology (GO) of the predicted targets was analyzed using functional items on Biological Process (<http://www.geneontology.org>). All gene definitions and functions were based on the National Institutes of Health databases (<http://www.ncbi.nlm.nih.gov/sites/entrez>). The GO covers three domains: Biological Process, Cellular Component, and Molecular Function. Fisher's exact test was used to find out if there was significant overlap between the differential expression (DE) list and the GO annotation list. The *P* value denotes the significance of GO term enrichment in the DE genes. Similarly, pathway analysis was used to find out the significant pathway of the predicted target genes according to the Kyoto Encyclopedia of Genes and Genomes (KEGG, <http://www.genome.jp/kegg/>). Likewise, the *P* value (EASE score, Fisher *P* value, or hypergeometric *P* value) denotes the significance of the pathway correlated to the conditions. The

threshold of significance was defined by  $P$  value and false discovery rate (FDR).

### Recombinant Plasmid Construction and Dual Luciferase Reported Assay

The 3'UTR of the *Mcl-1* mRNA which contains the target site for miR-106b-5p was amplified using real-time PCR and then introduced to the downstream of the Luciferase reporter gene in the Xba I (a DNA restriction endonuclease) cloning sites of the pGL3 control vector according to standard procedures (Promega, Madison, WI, USA). Plasmid DNA was subsequently isolated from recombinant colonies and sequenced to ensure the authenticity and direction of the inserted *Mcl-1* 3'UTR.

For the luciferase reporter assays, the PC12 cells were grown in DMEM with 10 % FBS to 70 % confluence in 24-well plates. The PC12 cells were co-transfected with 200 ng of firefly luciferase reporter vector containing the *Mcl-1* 3'UTR (named pGL3-*Mcl-1*-3'UTR), and 50 nmol/L mimic miR-106b-5p or 50 nmol/L mimic control (Genepharma) using Lipofectamine RNAiMAX™ transfection reagent (Invitrogen). Similarly, the PC12 cells were also co-transfected with 200 ng of pGL3-*Mcl-1*-3'UTR firefly luciferase reporter vector and 100 nmol/L inhibitor miR-106b-5p or 100 nmol/L inhibitor control (Genepharma). Twenty nanograms of pRL-TK vector (Promega) was co-transfected as internal control for normalization of the transfection efficiency. After 48 h, the transfected cells were harvested with ice-cold phosphate-buffered saline, and dual luciferase assay was performed according to the manufacturer's protocol (Promega). All the experiments were performed in triplicate.

### Western Blot Analysis

After the indicated treatment, the PC12 cells and rats' cerebral cortex were collected, washed with PBS, and homogenized in ice-cold RIPA buffer: 50 mmol/L Tris, pH 7.5; 150 mmol/L NaCl; 1 % NP-40; 0.5 % NaDOC; 0.1 % sodium dodecyl sulfate (SDS); and 1 mmol/L ethylene diamine tetraacetic acid (EDTA) that contained mini complete protease inhibitor cocktail (Sigma) and phosphatase inhibitors (Sigma). The lysed cells and tissues were centrifuged at 16,000g for 30 min at 4 °C. After the protein concentration measurement with the BCA protein assay kit (Biouniquer Technology), equal amounts of protein (50 µg) were separated by electrophoresis on 10 % sodium dodecyl sulfate polyacrylamide gels (SDS-PAGE) and transferred onto polyvinylidene difluoride (PVDF) membranes (Immobilon P, Millipore Corp., Billerica, MA). These membranes were incubated with 5 % (w/v) non-fat milk powder in Tris-buffered saline containing 0.1 % (v/v) Tween-20 (TBST) for 2 h to block nonspecific binding sites. The membranes were then incubated overnight

with gentle agitation at 4 °C with rabbit anti-Mcl-1 (1:200; Santa Cruz Biotechnology), anti-SOD-2 (1:1000; Cell Signaling Technology, Beverly, MA, USA), and β-actin (1:4000; Cell Signaling Technology). After having been washed with TBST, the membranes were incubated for 1 h at RT with HRP-conjugated goat anti-rabbit secondary antibody (1:3000; Cell Signaling Technology). The membranes were washed three times with TBST and developed using enhanced chemiluminescence (ECL) reagent (Amersham, Little Chalfont, UK). The intensity of the bands was measured using Gel Doc™ XR+ System (Bio-Rad Laboratories, Hercules, CA, USA). These values were then normalized to the corresponding control. All the experiments were repeated at least three times.

### Statistical Analysis

All cell culture data represent at least three independent experiments. All values are reported as mean ± SEM (standard error of the mean). Statistical significance was determined using  $t$  test to compare two groups or one-way analysis of variance (ANOVA) followed by Tukey's multiple comparison test for multiple comparisons. For correlation analyses, we used the Pearson correlation test. Statistical analysis was performed using GraphPad Prism 5 (GraphPad Software, San Diego, CA, USA). A  $P$  value of less than 0.05 was considered to be statistically significant.

## Results

### MiR-106b-5p Expression Levels in Cerebral Cortex of MCAO Rats and Glutamate-Treated PC12 Cells

Using miRNA microarray, our previous results have shown that a variety of miRNAs including miR-106b-5p exhibited significant differential expression in acute IS serum [10]. To date, the role of miR-106b-5p in stroke remains largely unknown. In the present study, we want to determine the miR-106b-5p expression status in the cerebral cortex of MCAO rats and the PC12 cell injury model. Firstly, we established the rat MCAO model and found that miR-106b-5p expression significantly increased in the infarct region of rats with 2 h MCAO/24 h reperfusion when compared with that of the sham group (Fig. 1a;  $P < 0.01$ ). To verify this finding in vitro, the glutamate-induced PC12 cell injury model, a popular neuronal cell injury model in vitro, was harnessed. As shown in Fig. 1b, miR-106b-5p was markedly upregulated after 4 h post glutamate treatment, while its level was not significantly changed in the PC12 cells during 8, 12, and 24 h glutamate treatment ( $P > 0.05$ ), respectively. To sum up, these in vivo and in vitro data suggest miR-106b-5p was induced in ischemic injury.

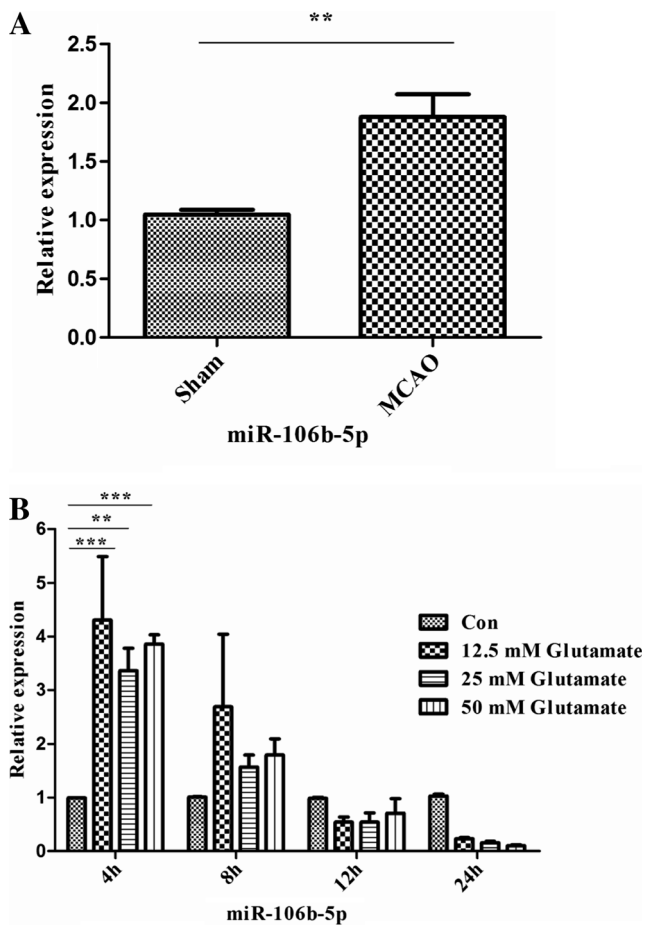


**Fig. 1** MiR-106b-5p expression in the MCAO rats' cerebral cortex and glutamate-induced PC12 cells. **a** MiR-106b-5p levels in MCAO rats' cerebral cortex were determined by real-time PCR after 24 h of reperfusion ( $n=6$  in each group), with U6 small RNA used as internal control. Values represent mean  $\pm$  SEM. Two asterisks  $P < 0.01$  show significant difference. **b** Glutamate induces miR-106b-5p expression in PC12 cells. PC12 cells were seeded on 12-well plates in complete medium for 24 h prior to exposure to glutamate at different concentrations (12.5, 25, 50 mmol/L) and for different times (4, 8, 12, 24 h). Data represent the mean  $\pm$  SEM. Two asterisks  $P < 0.01$  and three asterisks  $P < 0.001$  show significant differences. Con control, mM mmol/L

### MiR-106b-5p Enhanced Glutamate-Induced Apoptosis

Next, to explore the role of miR-106b-5p in glutamate-induced apoptosis, the PC12 cells were transfected with the miR-106b-5p mimic or miR-106b-5p inhibitor and their corresponding negative control. As shown in Fig. 2a, the PC12 cells treated with the miR-106b-5p mimic for 48 h exhibited the typical characteristics of apoptosis, including the condensation of chromatin and shrinkage of nuclear. Treatment of the PC12 cells with the miR-106b-5p inhibitor, however, considerably suppressed the glutamate-induced apoptotic cells with nuclear condensation and fragmentation. Similarly, flow cytometry analysis showed that the miR-106b-5p mimic increased the apoptosis percentage in the glutamate-induced

**Fig. 2** MiR-106b-5p increases glutamate-induced PC12 cell apoptosis. **a** Morphological observation of PC12 cells was performed by a phase-contrast microscope (magnification  $\times 200$ ). **b, c** Apoptosis rate was determined by flow cytometry analysis. All data are expressed as mean  $\pm$  SEM. Three asterisks  $P < 0.001$  represent significant differences

PC12 cells, which was effectively abrogated by the miR-106b-5p inhibitor (Fig. 2b, c;  $P < 0.001$ ).

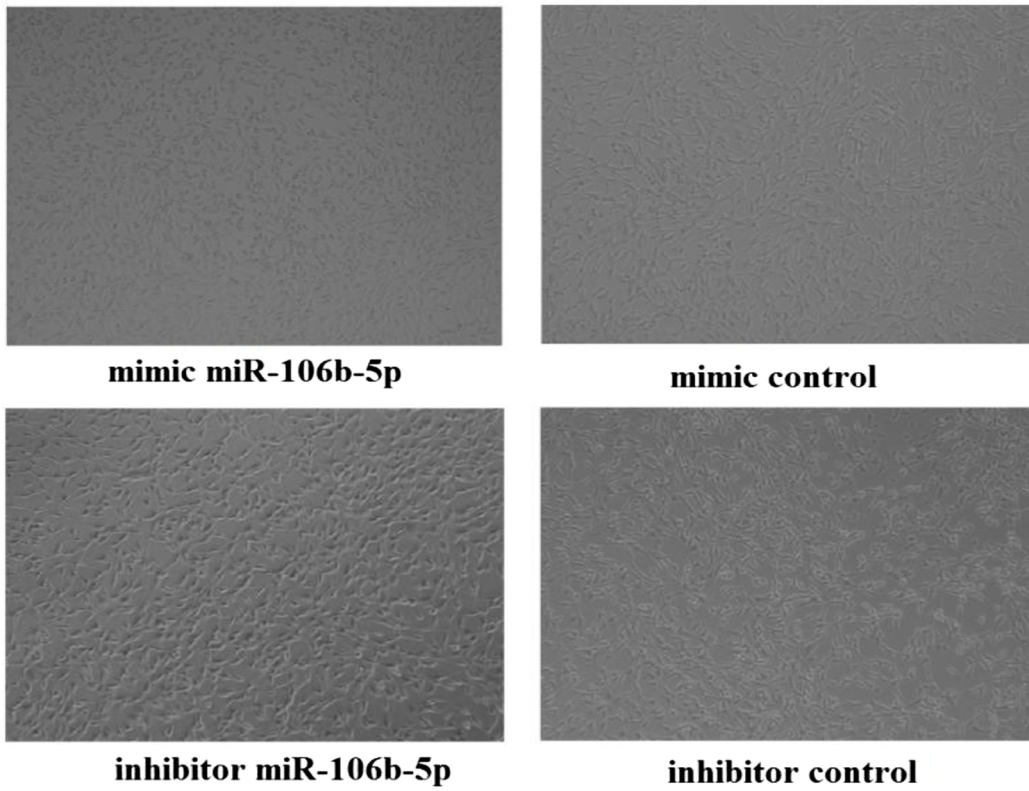
Meanwhile, the LDH release assay was performed as another indicator of cell toxicity. As shown in Fig. 3a, the miR-106b-5p mimic increased glutamate-evoked LDH release significantly relative to the negative control group, but the level was attenuated by miR-106b-5p inhibitor treatment ( $P < 0.05$ ,  $P < 0.01$ ), implying that miR-106b-5p may regulate the apoptosis of the glutamate-induced PC12 cells.

It is well known that the Bcl-2 family proteins, including Bcl-2, Bcl-xL, and Bax, play pivotal roles in regulating the mitochondria-mediated apoptotic pathway. The survival rate of neurons is determined by the balance between pro-apoptotic (Bax) and anti-apoptotic (Bcl-2) proteins during cerebral ischemia [2]. In addition, the increase in brain damage is associated with increased apoptosis as indicated by increased levels of Bax and decreased levels of Bcl-2. To confirm whether Bcl-2 and Bax participate in the process of miR-106b-5p-induced PC12 cell death, their levels were examined by real-time PCR analysis. A remarkable reduction in *Bax* mRNA levels in the PC12 cell was visible by miR-106b-5p inhibitor (Fig. 3b). Opposite changes were observed for *Bcl-2* mRNA expression, which was markedly elevated in the miR-106b-5p inhibitor group as compared with the inhibitor negative control group (Fig. 3c). In summary, these results indicate that downregulation of miR-106b-5p can protect PC12 cells against damage induced by glutamate.

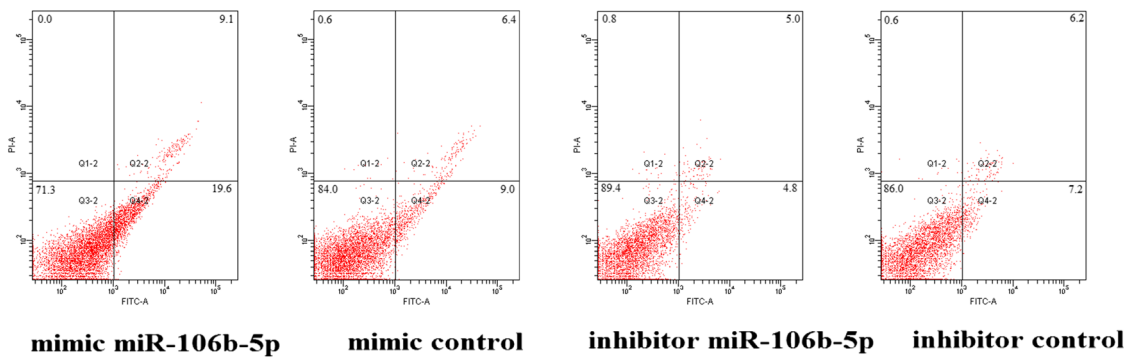
### MiR-106b-5p Regulated the Expression of Marker of Oxidative Stress: SOD and MDA

It is known that oxidative stress occurs in I/R injury. In regard to the anti-oxidative defense mechanism, SOD has the abilities to alleviate oxidative damage caused by ischemia/reperfusion (I/R) [26]. As shown in Fig. 4a, treatment with the miR-106b-5p mimic caused decreased SOD activity ( $P < 0.001$ ). In contrast, treatment with the miR-106b-5p inhibitor markedly increased SOD activity induced by glutamate ( $P < 0.05$ ). Additionally, the significant increase of the MDA (lipid peroxidation marker) level in PC12 cells transfected with the miR-106b-5p mimic was observed compared with the control group (Fig. 4b;  $P < 0.05$ ). However, treatment with the miR-106b-5p inhibitor significantly attenuated the increasing trends. The Western blot assay also showed that the miR-106b-5p mimic significantly decreased SOD-2 protein, while the

**A**



**B**



**C**

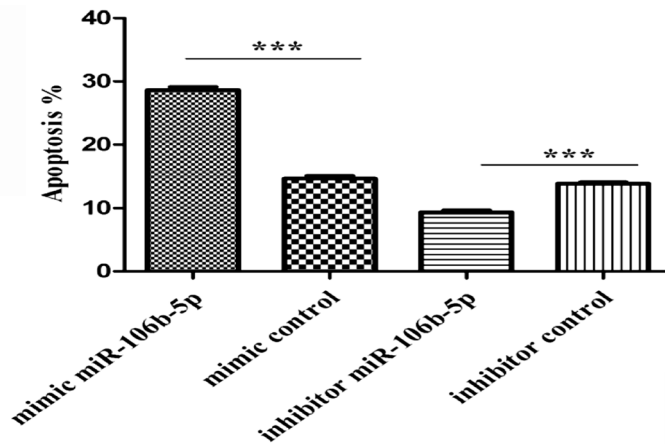
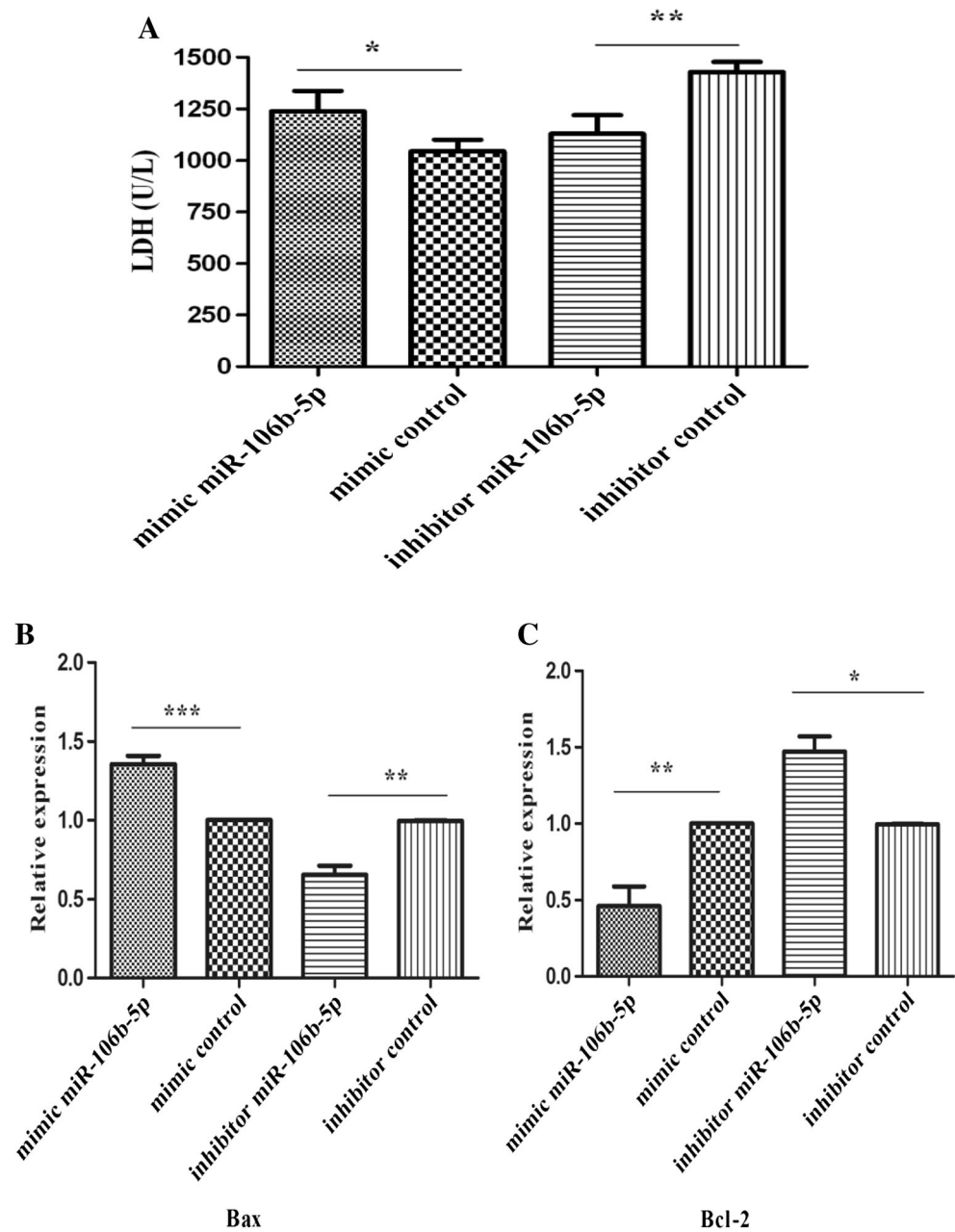


**Fig. 3** MiR-106b-5p increases expression of *Bax* and decreases expression of *Bcl-2* in glutamate-treated PC12 cells. **a** LDH release in PC12 cells. PC12 cells were pretreated with miR-106b-5p mimic, miR-106b-5p inhibitor, and the respective negative control, respectively, for 48 h and then incubated with glutamate (12.5 mmol/L) for 4 h. **b, c** MiR-106b-5p increased *Bax* mRNA levels and decreased *Bcl-2* mRNA levels after 48 h of miR-106b-5p treatment as indicated by real-time PCR assays. Values shown are mean  $\pm$  SEM. One asterisk  $P < 0.05$ , two asterisks  $P < 0.01$ , and three asterisks  $P < 0.001$  represent significant differences



inhibitor of miR-106b-5p remarkably upregulated SOD-2 protein (Fig. 4c, d;  $P < 0.05$ ,  $P < 0.001$ ), when compared with their respective negative control. Collectively, these results reveal the novel role of miR-106b-5p in regulating oxidative stress.

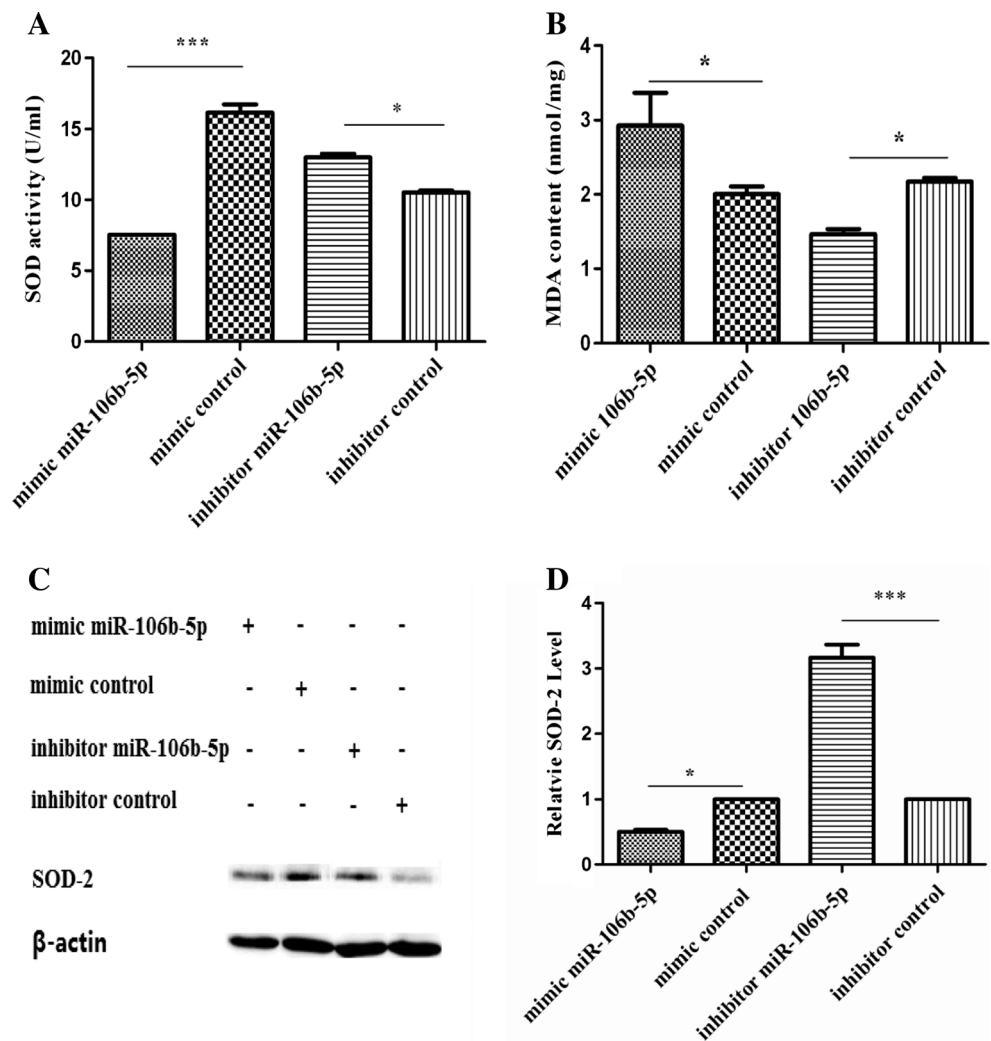
#### Downregulation of MiR-106b-5p Ameliorated the Neurological Deficits After I/R in Rats

To gain an insight into the possible effects of miR-106b-5p in I/R injury in vivo, we performed MCAO in male SD rats. When reperfusion initiates, the MCAO model group rats

received a vein injection of miR-106b-5p antagonist or antagonist negative control. After 24 h of reperfusion, neurological scores were tested. Treatment with the vein injection of miR-106b-5p antagonist resulted in significant knockdown of miR-106b-5p to ~50 % of control values (Fig. 5a;  $P < 0.05$ ). Obviously, neurological deficit scores significantly increased in the MCAO group (Fig. 5b;  $P < 0.05$ ). MiR-106b-5p antagonist treatment dramatically improved the neurological score in comparison with the miR-106b-5p antagonist control group (Fig. 5b;  $P < 0.05$ ). There was no statistical difference in the score between the antagonist control and MCAO groups (Fig. 5b;  $P > 0.05$ ).



**Fig. 4** MiR-106b-5p reduces SOD activity and upregulates MDA content in PC12 cells. PC12 cells were pretreated with miR-106b-5p mimic, miR-106b-5p inhibitor, and respective negative control for 48 h, respectively, and then incubated with glutamate (12.5 mmol/L) for 4 h. **a** SOD activity in PC12 cells. **b** MDA content in PC12 cells. **c** SOD-2 protein level in PC12 cells, as determined by Western blot. **d** Band intensities normalized to  $\beta$ -actin are represented. Values represent mean  $\pm$  SEM. *One asterisk*  $P < 0.05$  and *three asterisks*  $P < 0.001$  represent significant differences



### Downregulation of MiR-106b-5p Reduced Infarct Size in Ischemic Brains

The brain infarct size in the individual rats was evaluated by the 2,3,5-triphenyltetrazolium chloride (TTC) assay. Representative samples of TTC-stained brain sections are shown in Fig. 6a. Evidently, infarction was found in the MCAO group. MiR-106b-5p antagomir markedly decreased the infarction size of cortical infarction compared to the MCAO groups (Fig. 6b;  $P < 0.001$ ). However, the miR-106b-5p antagomir control had no significant effect on infarct size relative to the MCAO group (Fig. 6b;  $P > 0.05$ ).

MRI is considered the most promising and noninvasive approach for examining cerebral edema. Assessment of hemispheric volumes on MRI allows a direct quantification of the space-occupying effect in experimental stroke. The representative images are shown in Fig. 6c, and corresponding infarction volumes are shown in Fig. 6d. The MCAO group has clear hyperintensity and high infarct volumes. However, the infarct volumes were smaller in

the miR-106b-5p antagomir group than in the antagomir control group ( $P < 0.01$ ).

### Downregulation of MiR-106b-5p Attenuated Cerebral Damage

To evaluate the neuroprotective effect of miR-106b-5p antagomir on ischemic neuronal damages, we investigated the morphological changes of neuronal cells in the ischemic cortex of MCAO rats. Representative photomicrographs of HE staining are shown in Fig. 7. In the sham group, neuronal cells were normally intact and well-arranged morphologically with abundant cytoplasm and a clear nucleus in the cortex of rats. In contrast, in the MCAO and antagomir control groups, the neurons were markedly shrinking, degenerated, and necrotic, and their arrangement was disordered. However, after administration of miR-106b-5p antagomir, the extent of damage was significantly diminished, and the number of normal neurons significantly increased as well.

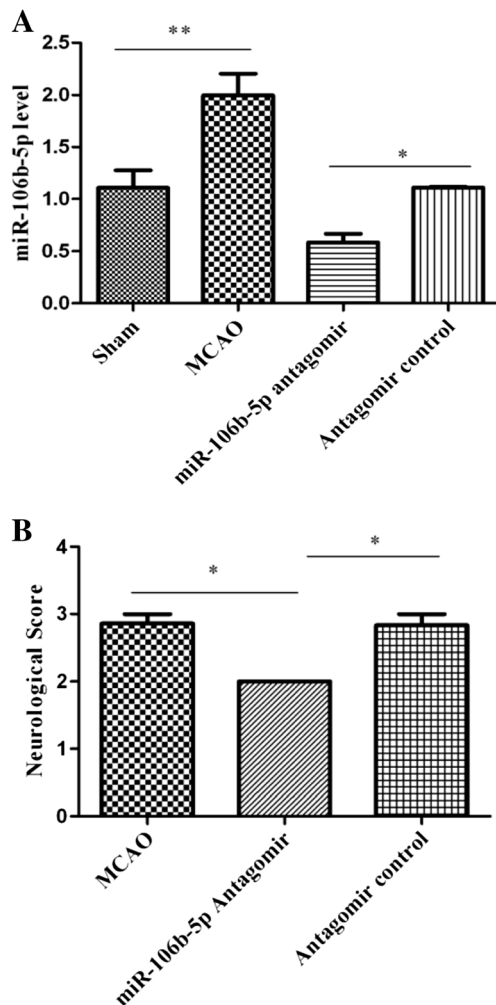


**Fig. 5** MiR-106b-5p antagomir ameliorated the neurological deficits after I/R in rats. Rats were subjected to 2 h of MCAO and then treated with miR-106b-5p antagomir or antagomir control for 24 h of reperfusion via tail vein. **a** MiR-106b-5p levels in ischemic cortex decrease with miR-106b-5p antagomir, relative to antagomir control. **b** Neurological deficit scores were assessed after 24 h of reperfusion ( $n = 6$  in each group). Data were expressed as mean  $\pm$  SEM. One asterisk  $P < 0.05$  and two asterisks  $P < 0.01$  represent significant differences

From these results, we can deduce that miR-106b-5p attenuates cerebral I/R injury.

### Downregulation of MiR-106b-5p Inhibits Apoptosis Following Cerebral I/R

Given the markedly improved recovery of brain function in the miR-106b-5p antagomir-injected rats, we next explored the effects of miR-106b-5p on apoptosis regulatory molecules and oxidative stress-related factors to clarify the possible neuroprotective mechanisms. We found that the expression of *Bax* mRNA was evidently decreased in the miR-106b-5p antagomir-treated group (Fig. 8a;  $P < 0.01$ ). We further analyzed the protein expression status of Bax in the cortex. As shown in Fig. 8b, c, the mean optical density of Bax-positive

cells increased in the ischemic cerebral cortex of the MCAO rats compared with the sham group. In addition, the mean optical density of Bax-positive cells was significantly reduced in the miR-106b-5p antagomir-injected rats relative to the negative controls.

Conversely, the expression of *Bcl-2* mRNA was significantly higher in the miR-106b-5p antagomir-treated group compared to the antagomir control group (Fig. 9a;  $P < 0.01$ ). The mean optical density of Bcl-2-positive cells was obviously higher in the miR-106b-5p antagomir-injected rats (Fig. 9b, c).

### Downregulation of MiR-106b-5p Upregulates Antioxidant Systems Following Cerebral I/R

To investigate the effect of miR-106b-5p on oxidative stress in vivo, SOD-2 expression in the cerebral cortex was assessed by Western blot. SOD-2 protein levels decreased in the MCAO groups compared to the sham groups but were upregulated by miR-106b-5p antagomir treatment (Fig. 10a, b), although there was no significant difference of SOD-2 protein levels between the MCAO and miR-106b-5p antagomir groups. In addition, SOD activity in the cortex was decreased in the MCAO group compared with that of the sham group, which was restored by miR-106b-5p antagomir (Fig. 10c). The MDA level in the cortex significantly increased in the MCAO group compared with that of the sham-operated group. An evident reduction of the MDA level was observed in the miR-106b-5p antagomir group compared with the antagomir control group (Fig. 10d;  $P < 0.05$ ).

### MiR-106b-5p Targets Mcl-1

To determine the possible targets of miR-106b-5p, miR-106b-5p-targeted genes were first predicted using miRBase, TargetScan, and miRanda. Then, GO and KEGG pathway analyses were applied to acquire their biological meanings. As a result, we found that miR-106b-5p could regulate a large number of genes and biological processes. There were 1097, 1220, and 4086 miR-106b-5p-target pairs in the miRBase, TargetScan, and miRanda programs, respectively (Fig. 11a). Moreover, 107 genes were present in all three programs. Interestingly, we saw enrichment for genes implicated in important biological processes, such as cellular response to stress, cellular metabolic process, positive regulation of the cellular process, etc (Fig. 11b). Moreover, these targets are significantly enriched in axon guidance, glutamatergic synapse, neurotrophin signaling pathway, etc. (Fig. 11c).

With bioinformatics sequence analysis, we found a binding site of miR-106b-5p seed region both in *Rattus norvegicus* and *Homo sapiens Mcl-1* mRNA 3'UTR with high possibility ranking (Fig. 12a). To confirm whether miR-106b-5p directly recognizes the 3'UTR of *Mcl-1* mRNA to repress its transcription or translation, we constructed a luciferase reporter vector,

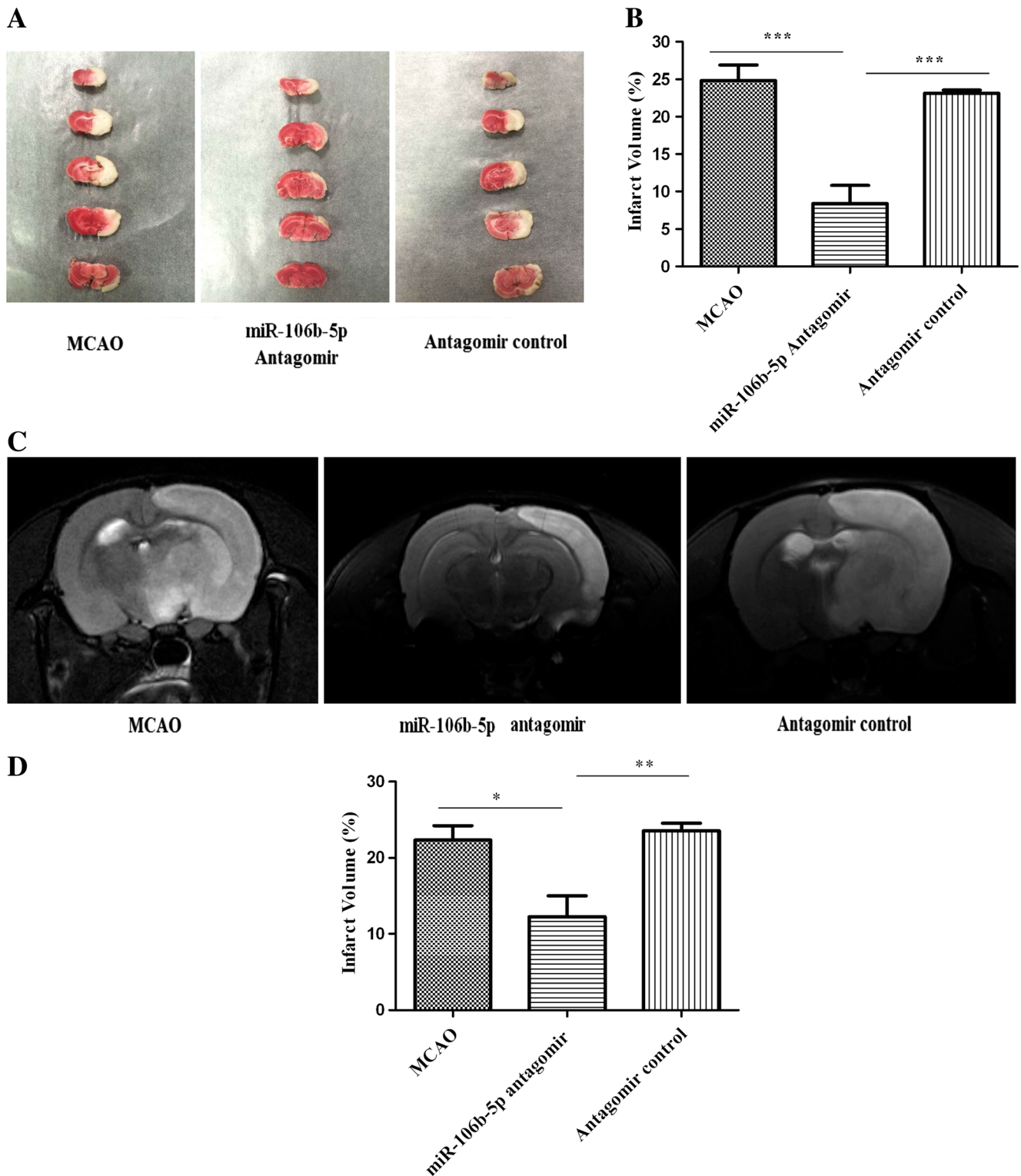


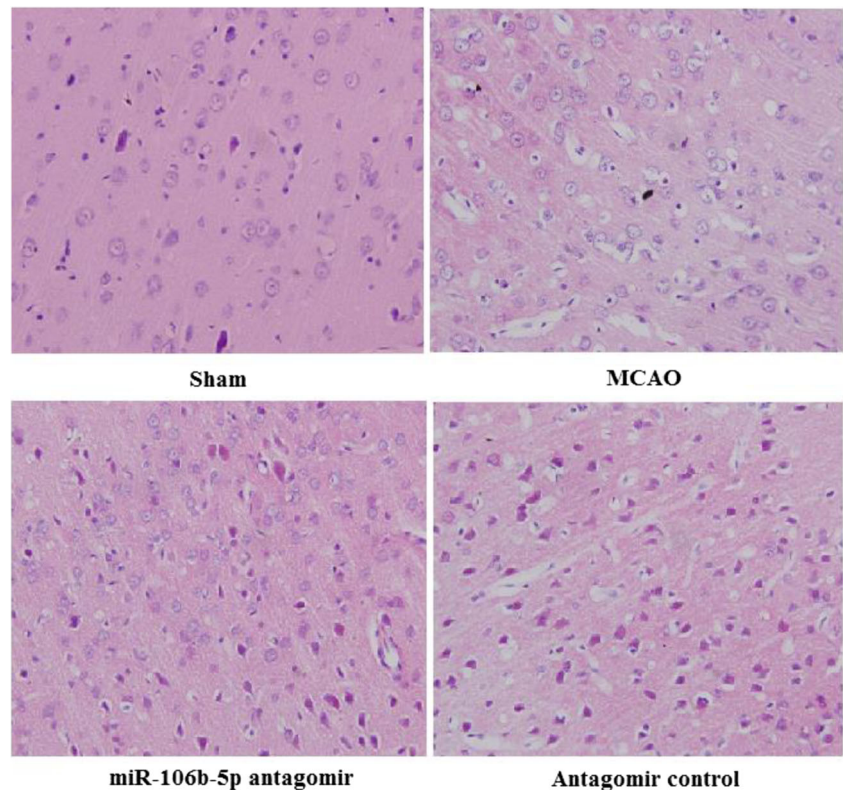
**Fig. 6** MiR-106b-5p antagonist reduced infarct size in ischemic brains. **a** Representative pictures of TTC staining of cerebral infarct size in brain sections ( $n = 6$  in each group). The infarcted tissue remained unstained (white), whereas normal brain tissues were stained red. **b** Quantification of infarct size by TTC staining after 24 h of reperfusion. **c** MRI images on

T2-weighted images (T2WI) in MCAO group, miR-106b-5p antagomir group, and antagomir control group. **d** Quantification of infarct size by MRI after 24 h of reperfusion. Data were expressed as mean  $\pm$  SEM. One asterisk  $P < 0.05$ , two asterisks  $P < 0.01$ , and three asterisks  $P < 0.001$  represent significant differences

which was followed by a fragment of the 3'UTR from *Mcl-1* mRNA containing the predicted miR-106b-5p binding

sequences. The luciferase activity assay indicated that the miR-106b-5p mimic significantly decreased the luciferase

**Fig. 7** MiR-106b-5p antagomir attenuated cerebral damage. Representative images of histological assay of rats' ischemic cortex in different groups (magnification  $\times 400$ )



activity of the reporter vector containing miR-106b-5p binding sequences of *Mcl-1* mRNA 3'UTR (Fig. 12b;  $P < 0.001$ ). Furthermore, the miR-106b-5p mimic and miR-106b-5p inhibitor could down- and upregulate both *Mcl-1* mRNA (Fig. 12c) and protein expression levels in PC12 cells, respectively (Fig. 12d, e). These results suggest that miR-106b-5p can directly recognize the 3'UTR of *Mcl-1* mRNA to negatively regulate Mcl-1 protein levels through promoting degradation of its mRNA.

#### Downregulation of MiR-106b-5p Upregulates Expression of Mcl-1 in Ischemic Cortex

Considering that Mcl-1 was the target of miR-106b-5p, we evaluated the effect of miR-106b-5p on the expression of Mcl-1 in vivo. As expected, *Mcl-1* increased markedly in the miR-106b-5p antagomir group (Fig. 13a). The expression of Mcl-1 protein was detected in different groups in further investigation. From the Western blot analysis, Mcl-1 protein was downregulated after cerebral I/R injury (Fig. 13b, c;  $P < 0.001$ ). However, these changes were remarkably reversed by miR-106b-5p antagomir ( $P < 0.05$ ).

Next, we explored the correlation between the *miR-106b-5p* expression level and mRNA levels of *Mcl-1* in the ischemic cortex. After normalization, RNA levels of *miR-106b-5p* and mRNA levels of *Mcl-1* were analyzed by Pearson's correlation coefficient analysis. Markedly, the results indicated an

inverse correlation between *miR-106b-5p* and *Mcl-1* expression levels in the ischemic cortex (Fig. 13d;  $R = -0.8543$ ,  $P < 0.05$ ). Collectively, these results imply that endogenous levels of *Mcl-1* in the cortex can be negatively regulated by *miR-106b-5p*. In summary, it is noteworthy that the functional involvement of upregulation of miR-106b-5p in dysregulating apoptosis and oxidative stress may lead to the onset of I/R injury (Fig. 13e).

#### Discussion

In the present study, we identified the upregulation of miR-106b-5p as a major contributor to cerebral ischemic injury. Our results illustrated that miR-106b-5p may have the potential to regulate apoptosis and oxidative stress. This observation highlighted the functional significance of miR-106b-5p in influencing brain damage outcomes.

Neuronal damage after I/R was induced by oxidative stress and mitochondrial dysfunction that ultimately resulted in an apoptotic cascade [2]. The genes responsible for IS-induced neuronal cell apoptosis have not been fully identified, although various studies have sought to elucidate the molecular basis of acute IS. It is well known that the increase in brain damage is associated with increased apoptosis as indicated by increased levels of Bax and decreased levels of Bcl-2. Our data indicated that a great number of apoptotic cells were found in the MCAO rats' brain at 24 h after reperfusion and

**Fig. 8** MiR-106b-5p antagomir inhibits the expression of Bax following cerebral I/R. **a** Real-time PCR shows the mRNA expression of *Bax* in cortex from the sham, MCAO, miR-106b-5p antagomir, and antagomir control groups after 24 h of reperfusion ( $n = 6$  in each group).  $\beta$ -Actin was used as an internal control. **b** Immunohistochemistry staining for Bax in rats' cortex (magnification  $\times 400$ ). **c** Mean optical density of the Bax immunopositive cells in rats' cortex. Data are expressed as mean  $\pm$  SEM. *One asterisk*  $P < 0.05$  and *two asterisks*  $P < 0.01$  represent significant differences

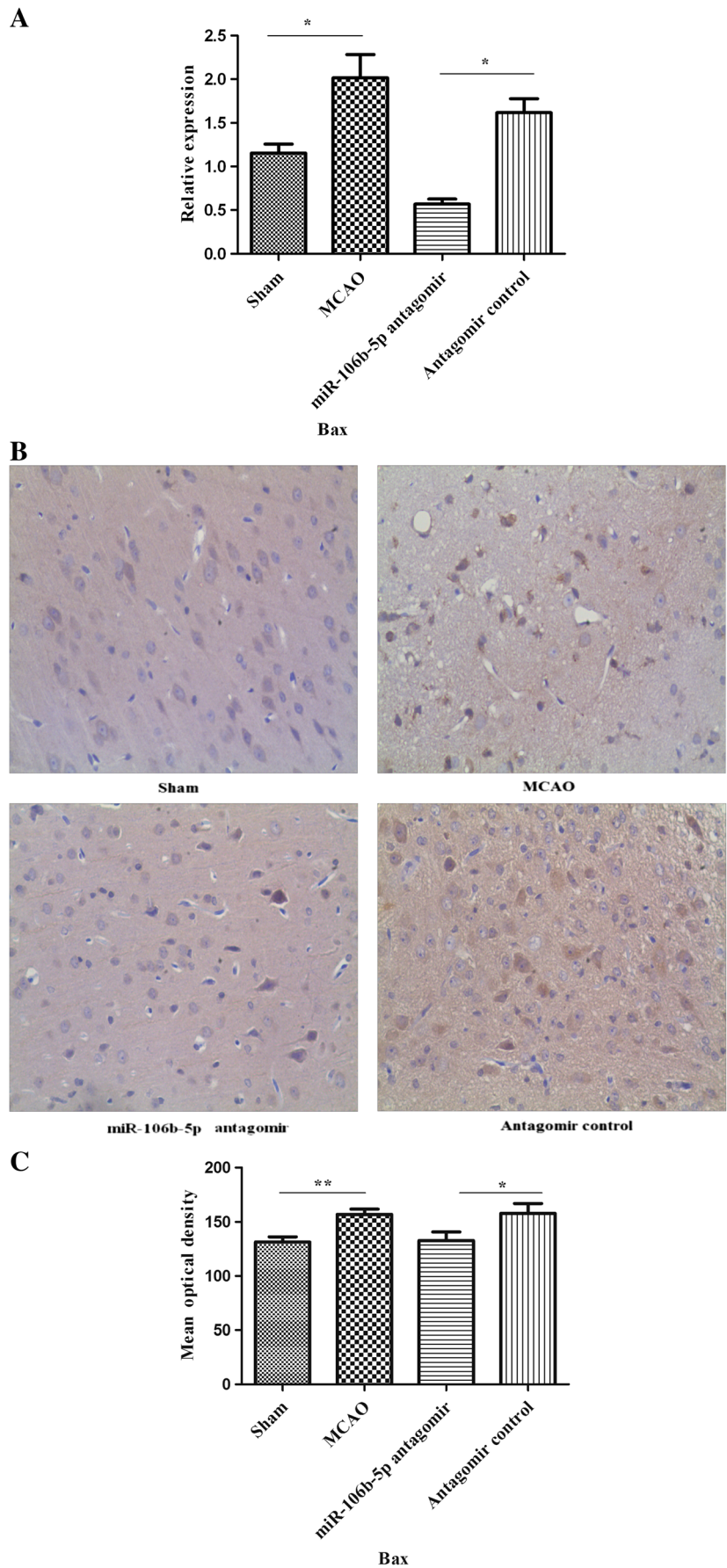


**Fig. 9** MiR-106b-5p antagomir upregulates the expression of Bcl-2 following cerebral I/R. **a** Real-time PCR shows the mRNA expression of *Bcl-2* in cortex from the sham, MCAO, miR-106b-5p antagomir, and antagomir control groups after 24 h of reperfusion ( $n = 6$  in each group).  $\beta$ -Actin was used as an internal control. **b** Immunohistochemistry staining for Bcl-2 in rats' cortex (magnification  $\times 400$ ). **c** Mean optical density of the Bcl-2 immunopositive cells in rats' cortex. Data are expressed as mean  $\pm$  SEM. *One asterisk*  $P < 0.05$  and *two asterisks*  $P < 0.01$  represent significant differences

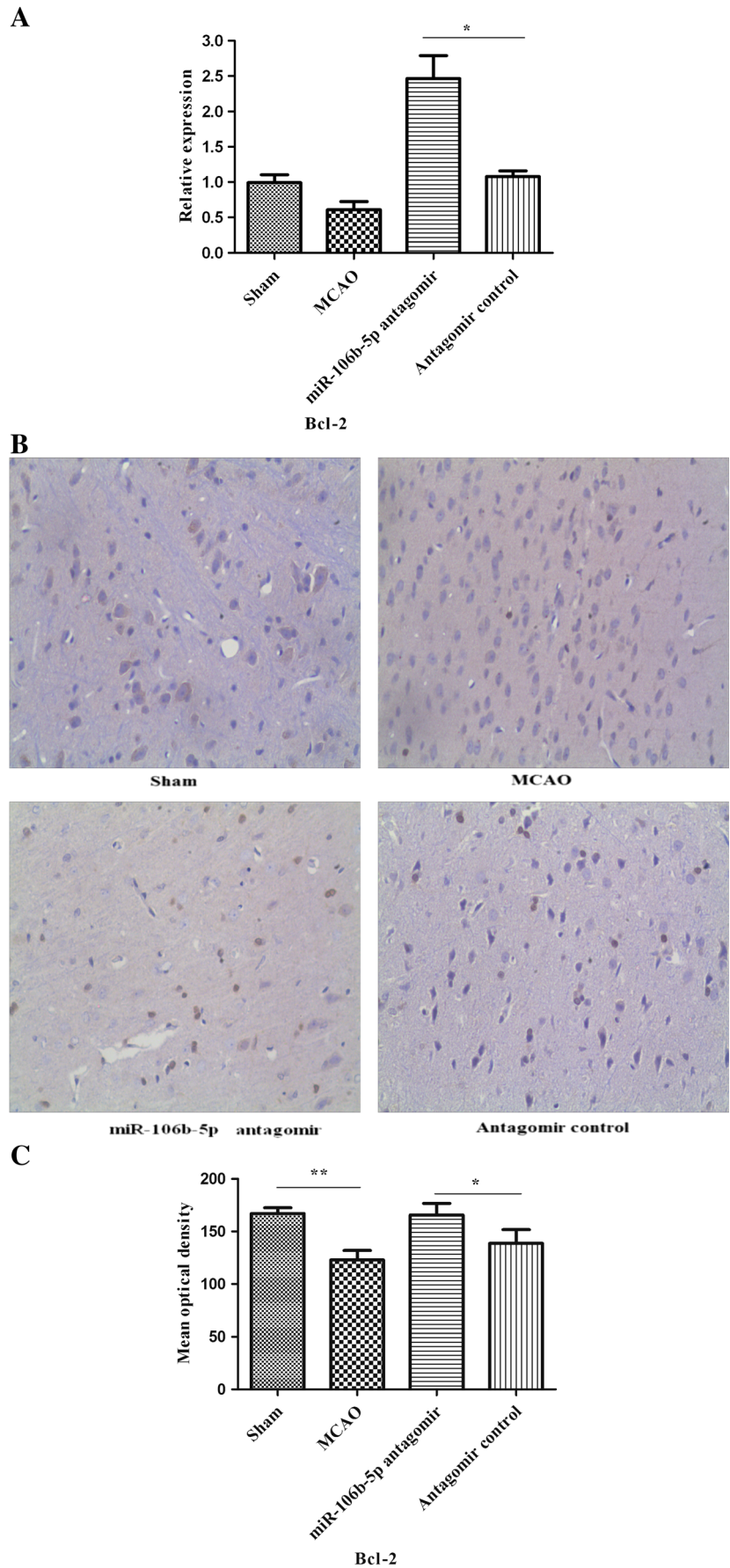
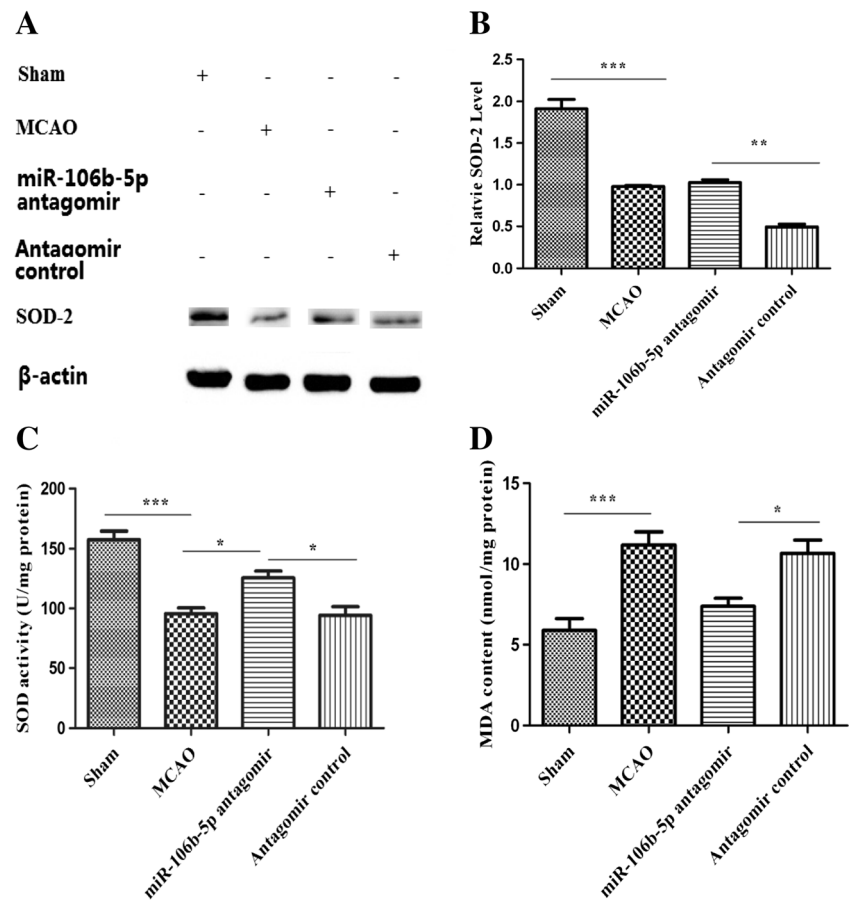


**Fig. 10** MiR-106b-5p antagomir upregulates antioxidant systems following cerebral I/R. **a** Protein levels of SOD-2 in cortex from sham, MCAO, miR-106b-5p antagomir, and antagomir control groups were measured by Western blot. **b** Band intensities normalized to  $\beta$ -actin are represented. **c, d** Histograms showed the activity of SOD and concentration of MDA in cortex homogenates. Data represent mean  $\pm$  SEM. *One asterisk*  $P < 0.05$ , *two asterisks*  $P < 0.01$ , and *three asterisks*  $P < 0.001$  represent significant differences



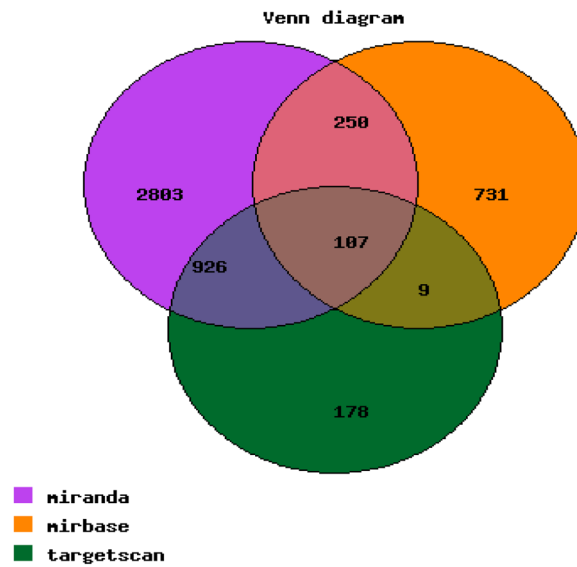
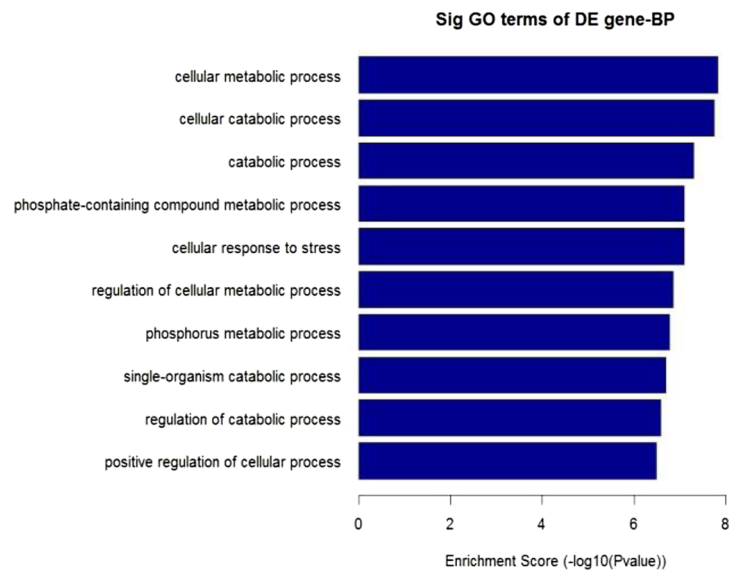
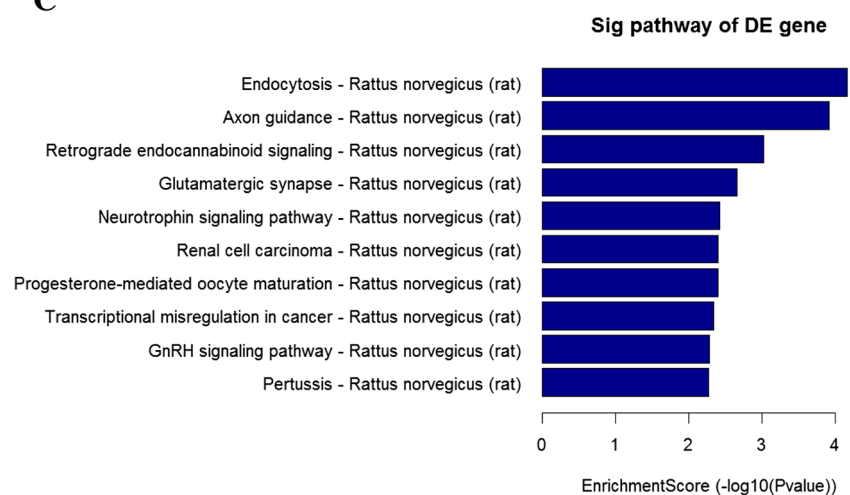
there was also a significant upregulation of Bax and downregulation of Bcl-2 in the MCAO rats' brain. This is consistent with previous reports regarding the production of apoptosis [27, 28]. Accumulating evidence showed that inhibition of apoptosis had a beneficial effect in an acute IS process. For example, antisense knockdown of endogenous *Bcl-2* mRNA exacerbated cerebral ischemic injury in rats and blocked the neuroprotection afforded by ischemic preconditioning [29, 30]. In this study, miR-106b-5p antagomir treatment reduced neuronal apoptosis. These results demonstrated that the neuroprotection of miR-106b-5p antagomir is probably through increasing expression levels of Bcl-2 and Mcl-1. Further studies are required to dissect the detailed mechanisms underlying the regulation of apoptosis by miR-106b-5p.

Impaired balance between products of oxidative stress and the levels of antioxidant enzyme activities might be the important mechanism underlying the occurrence of IS [31]. Free radicals and reactive oxygen species (ROS) are found excessively elevated during cerebral I/R, which results in oxidative stress. Studies reported that administration of antioxidants or upregulation of antioxidant enzyme activities could improve neurological deficit and attenuate neuron damage during ischemic I/R injury [32, 33]. To explore the possible mechanism of miR-106b-5p antagomir on the relief of oxidative stress

induced by I/R injury, we investigated the miR-106b-5p antagomir-dependent effects on MDA content and SOD activity in MCAO rat cortex tissue homogenates. Our results showed that miR-106b-5p antagomir significantly increased SOD activity and decreased MDA levels in the ischemic cerebral cortex. These data suggest that miR-106b-5p antagomir affords protection against cerebral I/R injury through the amelioration of oxidative stress. Thus, our results have provided evidence for miR-106b-5p antagomir's anti-oxidative activity after cerebral I/R.

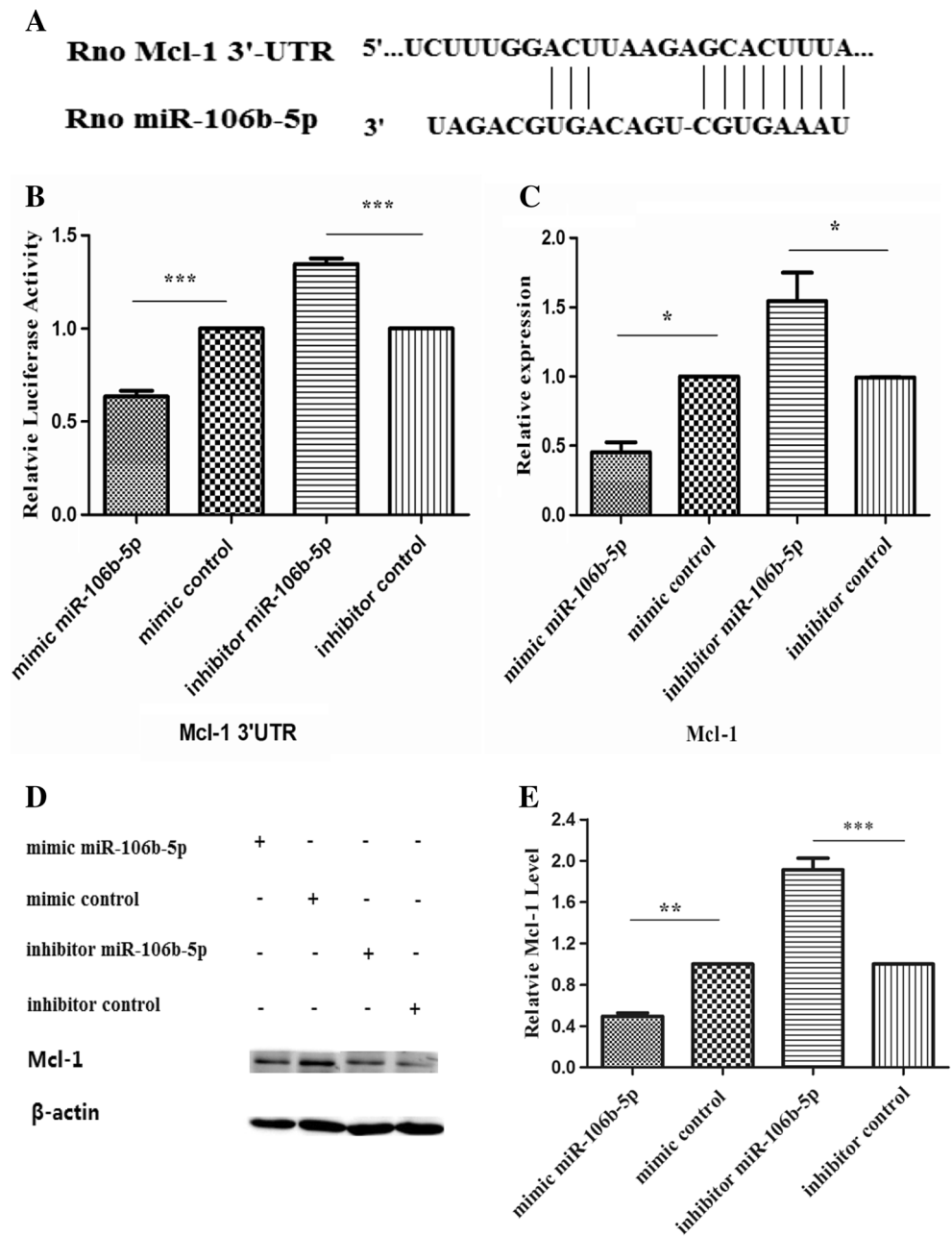
With informatics prediction and sequential experimental demonstration, Mcl-1 was identified as the direct target of miR-106b-5p in our study. Mcl-1, an anti-apoptotic member of the Bcl-2 family, is a key regulator of apoptosis during CNS development and after DNA damage [34, 35]. Mori et al. proved the neuroprotective role for Mcl-1 in seizure-induced neuronal death following pilocarpine-induced status epilepticus [36]. However, little was known about the expression and functions of Mcl-1 in the brain following cerebral ischemia. In the present study, high expression levels of Mcl-1 were observed to be associated with reduced levels of apoptosis in the antagomir miR-106b-5p-treated rats. It is reported that p38 MAPK activation reduced Mcl-1 expression in chronic lymphocytic leukemia [37]. We therefore hypothesized that miR-106b-5p may regulate

**Fig. 11** Function analysis of targets of miR-106b-5p. **a** A Venn diagram for prediction of targets of miR-106b-5p. Prediction of targets was performed by three different target prediction databases: miRBase (<http://www.ebi.ac.uk/enright-srv/microcosm>), TargetScan (<http://www.targetscan.org>), and miRanda (<http://www.microRNA.org>). **b** GO analysis was used to determine the probable biological function of the miR-106b-5p targets. GO of the predicted targets was analyzed using functional items on biological process (<http://www.geneontology.org>). **c** Pathway analysis was used to find out the significant pathway of the predicted target genes according to KEGG (<http://www.genome.jp/kegg/>). Likewise, the *P* value denotes the significance of the pathway correlated to the conditions

**A****B****C**



**Fig. 12** Mcl-1 is an authentic target of miR-106b-5p. **a** Predicted binding site of miR-106b-5p in the 3'UTR of *Mcl-1*. **b** Predicted binding for *miR-106b-5p*: *Mcl-1* 3'UTR was assessed by dual luciferase activity assay in PC12 cells co-transfected with firefly luciferase reporter vector and pRL-TK vector, plus either miR-106b-5p mimic or miR-106b-5p inhibitor. **c** Levels of *Mcl-1* mRNA in PC12 cells were detected by real-time PCR assay. **d** Protein expression of Mcl-1 in PC12 cells was detected by Western blot analysis. **e** Band intensities normalized to  $\beta$ -actin are represented. All cell culture experiments were performed in triplicate. Data represent mean  $\pm$  SEM. One asterisk  $P < 0.05$ , two asterisks  $P < 0.01$ , and three asterisks  $P < 0.001$  represent significant differences



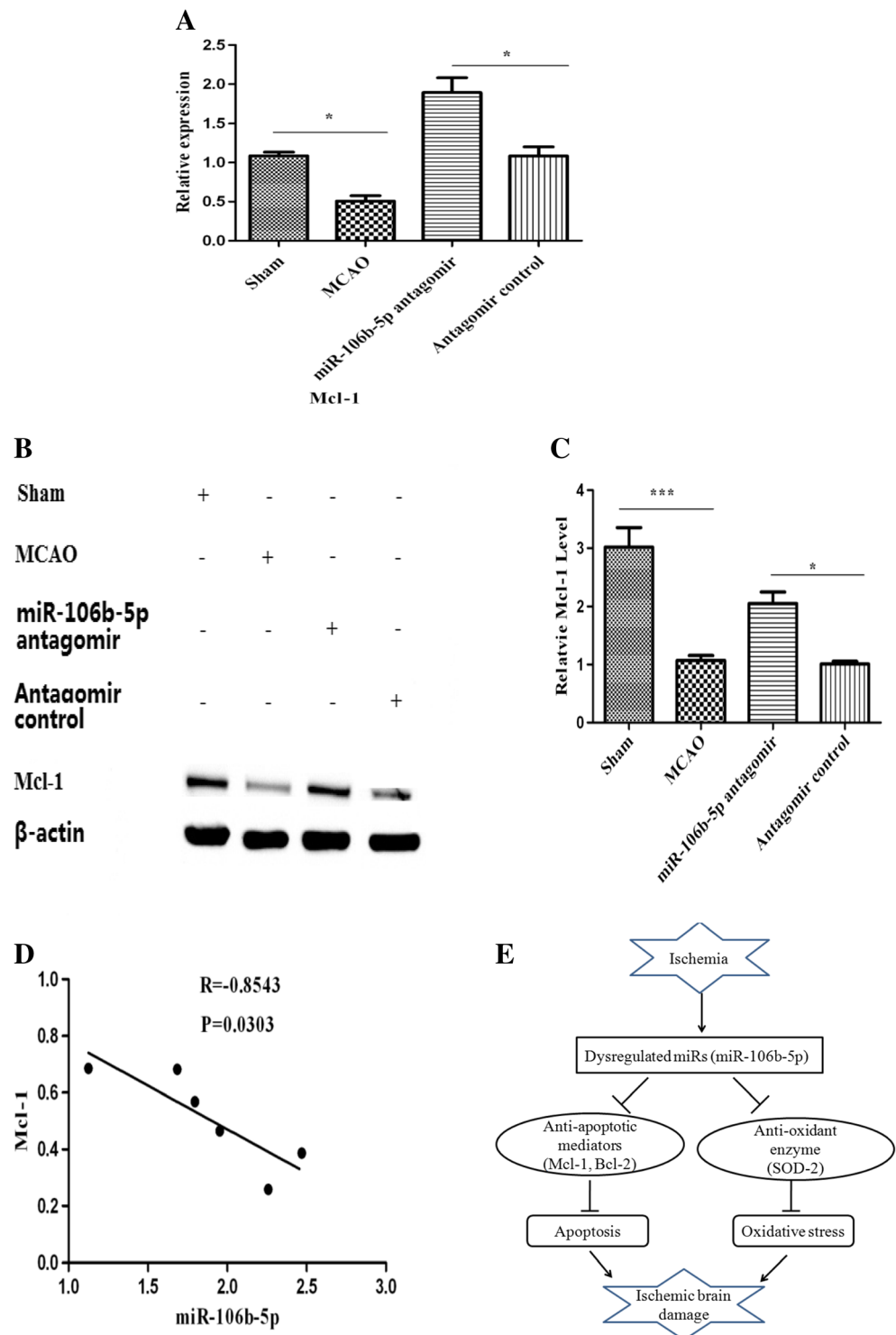
Mcl-1 expression directly or influence Mcl-1 expression via regulating the MAPK signaling pathway indirectly, but the exact mechanisms remain to be fully understood.

Some functionally validated target genes of miR-106b are implicated in cancer-related processes such as the cell cycle (E2F1, p21) [38, 39] and apoptosis (BCL2L11) [40]. Besides, miR-106b could promote neuronal differentiation of neural stem cells (NSC) in adults [41]. These results suggest a role for miR-106b in normal adult stem cells, in addition to a known role in cancer cells. Our data suggests that miR-106b-5p antagonist contributes to improvement in functional outcome. However, extra studies are required to confirm the influence of miR-106b-5p on the proliferation and differentiation of NSC

and neurogenesis. Moreover, additional targets of miR-106b-5p may be relevant for stroke. Future studies need to knock-down these targets to evaluate their relevance for protection.

Pathway analysis based on the KEGG pathway database indicated that targets of miR-106b-5p were significantly enriched in nervous system-related signaling pathways including axon guidance, glutamatergic synapse, neurotrophin signaling pathway, etc. In recent studies, emerging evidences highlight a role for miRNAs in spinal morphology and function during nervous system development [42]. MiR-21 enhances neurotrophin signaling and controls neuronal differentiation [43]. In addition, miR-101b could regulate synapse density, dendritic spine shape, and synaptic physiology [44].

**Fig. 13** MiR-106b-5p antagomir upregulates expression of Mcl-1 in ischemic cortex. **a** Real-time PCR shows the mRNA expression of *Mcl-1* in cortex from the sham, MCAO, miR-106b-5p antagomir, and antagomir control groups after 24 h of reperfusion ( $n = 6$  in each group). **b** Protein levels of Mcl-1 in cortex from sham, MCAO, miR-106b-5p antagomir, and antagomir control groups were measured by Western blot. **c** Band intensities normalized to  $\beta$ -actin are represented. **d** Pearson's correlation coefficient analysis between the expression levels of *miR-106b-5p* and *Mcl-1* in MCAO cortex. **e** The proposed model of miR-106b-5p-mediated I/R injury. Data are expressed as mean  $\pm$  SEM. *One asterisk*  $P < 0.05$  and *three asterisks*  $P < 0.001$  represent significant differences



Another report found that miR-204 together with other genes participated in the regulation of axon guidance [45]. Accordingly, our findings may provide important new information in the roles of miR-106b-5p in the control of axon guidance and more broadly in nervous system development.

A multitude of miRNAs appear in clusters on single polycistronic transcripts [46–48]. The miR-106b-25 cluster

encodes for three miRNAs: miR-106b, miR-93, and miR-25, which is embedded within the mini chromosome maintenance protein 7 (MCM7) gene. In prostate cancers, the expression of the miR-106b-25 cluster has been shown to correspond to that of MCM7 transcripts [49]. Hence, the transcription of the miR-106b-25 cluster is regulated via the expression of the MCM7 gene. What is more, both c-Myc and E2F1 have been

shown to upregulate MCM7 expression [50]. We took the attitude that glutamate induced the expression of miR-106b in a p38 MAPK-dependent manner (data not shown). Recent reports also revealed that p38 MAPK regulated MCM7 expression via collaborating with transcript factors such as c-Myc and E2F1 [51]. Therefore, we presume that glutamate induces the expression of miR-106b-5p through regulating MCM7 gene expression.

It is noted that in rat brains of MCAO, dozens of miRNAs were predicted to target genes that are involved in mediating numerous functions, including apoptosis, antioxidant, and neuroprotection. Among them, miR-200c contributes to brain cell death by inhibiting reelin expression [18]. Additionally, miR-497 promotes ischemic neuronal death by negatively regulating anti-apoptotic proteins, bcl-2 and bcl-w [20]. Interestingly, several recent reports also showed that miR-181a can directly target Bcl-2, X-linked inhibitor of apoptosis, and glucose-regulated protein 78 in astrocytes and increased neuronal survival [19, 52, 53]. It is a remarkable fact that miR-424 protects against transient cerebral I/R injury by inhibiting SOD activity [22]. Meanwhile, miR-145, induced by stroke, could target SOD-2 expression [54]. Our results manifested that miR-106b may regulate apoptosis-related and oxidative stress genes as well, such as Mcl-1 and SOD-2. Our findings extend the knowledge about miRNAs in stroke therapy. In addition, our group previously demonstrated a central role of ultrasound in protecting against cerebral I/R injury [55]. In the future, combination therapy of ultrasound and miR-106b-5p antagomir in stroke will be a beneficial try. Our results may provide new insight into therapeutic targets in stroke. If possible, additional work is required to study the role of miR-106b-5p in other neurological disorders such as Alzheimer's disease (AD), multiple sclerosis (MS), and Parkinson's disease (PD).

## Conclusions

Taken together, this study demonstrated that the neuroprotective effects of miR-106b-5p antagomir on MCAO rats were associated with attenuation of apoptosis and oxidative stress. Studies of the effects of miR-106b-5p on MCAO rats will be essential in further demonstrating the clinical relevance for the treatment of stroke.

**Acknowledgments** This work was supported by grants from the National Natural Science Foundation of China (Grant Nos. 81171659, 11574156, 81373748, and 81403136) and the 333 Project of Jiangsu Province in China (Grant No. BRA2014341). The funders had no role in the study design, data collection and analysis, decision to publish, or preparation of the manuscript.

**Compliance with Ethical Standards** This study was approved by the Animal Care and Use Committee of the Affiliated Hospital of Nanjing

University of Chinese Medicine. All procedures were performed in accordance with the pertinent guidelines. All efforts were made to minimize animal suffering and the number of animals employed.

**Conflict of Interest** The authors declare that they have no conflict of interest.

## References

- Goldstein LB, Adams R, Becker K, Furberg CD, Gorelick PB, Hademenos G, Hill M, Howard G, Howard VJ, Jacobs B, Levine SR, Mosca L, Sacco RL, Sherman DG, Wolf PA, del Zoppo GJ (2001) Primary prevention of ischemic stroke: a statement for healthcare professionals from the Stroke Council of the American Heart Association. *Stroke* 32(1):280–299
- Broughton BR, Reutens DC, Sobey CG (2009) Apoptotic mechanisms after cerebral ischemia. *Stroke* 40(5):e331–e339. doi:10.1161/STROKEAHA.108.531632
- Lagos-Quintana M, Rauhut R, Lendeckel W, Tuschl T (2001) Identification of novel genes coding for small expressed RNAs. *Science* 294(5543):853–858. doi:10.1126/science.1064921
- He L, Hannon GJ (2004) MicroRNAs: small RNAs with a big role in gene regulation. *Nat Rev Genet* 5(7):522–531. doi:10.1038/nrg1379
- Im HI, Kenny PJ (2012) MicroRNAs in neuronal function and dysfunction. *Trends Neurosci* 35(5):325–334. doi:10.1016/j.tins.2012.01.004
- Schratt GM, Tuebing F, Nigh EA, Kane CG, Sabatini ME, Kiebler M, Greenberg ME (2006) A brain-specific microRNA regulates dendritic spine development. *Nature* 439(7074):283–289. doi:10.1038/nature04367
- Lee ST, Chu K, Jung KH, Yoon HJ, Jeon D, Kang KM, Park KH, Bae EK, Kim M, Lee SK, Roh JK (2010) MicroRNAs induced during ischemic preconditioning. *Stroke* 41(8):1646–1651. doi:10.1161/STROKEAHA.110.579649
- Jeyaseelan K, Lim KY, Armugam A (2008) MicroRNA expression in the blood and brain of rats subjected to transient focal ischemia by middle cerebral artery occlusion. *Stroke* 39(3):959–966. doi:10.1161/STROKEAHA.107.500736
- Liu DZ, Tian Y, Ander BP, Xu H, Stamova BS, Zhan X, Turner RJ, Jickling G, Sharp FR (2010) Brain and blood microRNA expression profiling of ischemic stroke, intracerebral hemorrhage, and kainate seizures. *J Cereb Blood Flow Metab* 30(1):92–101. doi:10.1038/jcbfm.2009.186
- Li P, Teng F, Gao F, Zhang M, Wu J, Zhang C (2015) Identification of circulating microRNAs as potential biomarkers for detecting acute ischemic stroke. *Cell Mol Neurobiol* 35(3):433–447. doi:10.1007/s10571-014-0139-5
- Landais S, Landry S, Legault P, Rassart E (2007) Oncogenic potential of the miR-106-363 cluster and its implication in human T-cell leukemia. *Cancer Res* 67(12):5699–5707. doi:10.1158/0008-5472.CAN-06-4478
- Liu F, Gong J, Huang W, Wang Z, Wang M, Yang J, Wu C, Wu Z, Han B (2014) MicroRNA-106b-5p boosts glioma tumorigenesis by targeting multiple tumor suppressor genes. *Oncogene* 33(40):4813–4822. doi:10.1038/onc.2013.428
- Xiang W, He J, Huang C, Chen L, Tao D, Wu X, Wang M, Luo G, Xiao X, Zeng F, Jiang G (2015) miR-106b-5p targets tumor suppressor gene SETD2 to inactivate its function in clear cell renal cell carcinoma. *Oncotarget* 6(6):4066–4079
- Wang J, Yu JT, Tan L, Tian Y, Ma J, Tan CC, Wang HF, Liu Y, Tan MS, Jiang T, Tan L (2015) Genome-wide circulating microRNA

- expression profiling indicates biomarkers for epilepsy. *Sci Rep* 5: 9522. doi:10.1038/srep09522
15. Shiotani A, Murao T, Kimura Y, Matsumoto H, Kamada T, Kusunoki H, Inoue K, Uedo N, Iishi H, Haruma K (2013) Identification of serum miRNAs as novel non-invasive biomarkers for detection of high risk for early gastric cancer. *Br J Cancer* 109(9):2323–2330. doi:10.1038/bjc.2013.596
  16. Baraniskin A, Kuhnhen J, Schlegel U, Chan A, Deckert M, Gold R, Maghnouj A, Zollner H, Reinacher-Schick A, Schmiegel W, Hahn SA, Schroers R (2011) Identification of microRNAs in the cerebrospinal fluid as marker for primary diffuse large B-cell lymphoma of the central nervous system. *Blood* 117(11):3140–3146. doi:10.1182/blood-2010-09-308684
  17. Doepfner TR, Doehring M, Bretschneider E, Zechariah A, Kaltwasser B, Muller B, Koch JC, Bahr M, Hermann DM, Michel U (2013) MicroRNA-124 protects against focal cerebral ischemia via mechanisms involving Usp14-dependent REST degradation. *Acta Neuropathol* 126(2):251–265. doi:10.1007/s00401-013-1142-5
  18. Stary CM, Xu L, Sun X, Ouyang YB, White RE, Leong J, Li J, Xiong X, Giffard RG (2015) MicroRNA-200c contributes to injury from transient focal cerebral ischemia by targeting Reelin. *Stroke* 46(2):551–556. doi:10.1161/STROKEAHA.114.007041
  19. Moon JM, Xu L, Giffard RG (2013) Inhibition of microRNA-181 reduces forebrain ischemia-induced neuronal loss. *J Cereb Blood Flow Metab* 33(12):1976–1982. doi:10.1038/jcbfm.2013.157
  20. Yin KJ, Deng Z, Huang H, Hamblin M, Xie C, Zhang J, Chen YE (2010) miR-497 regulates neuronal death in mouse brain after transient focal cerebral ischemia. *Neurobiol Dis* 38(1):17–26. doi:10.1016/j.nbd.2009.12.021
  21. Khanna S, Rink C, Ghoorkhanian R, Gnyawali S, Heigel M, Wijesinghe DS, Chalfant CE, Chan YC, Banerjee J, Huang Y, Roy S, Sen CK (2013) Loss of miR-29b following acute ischemic stroke contributes to neural cell death and infarct size. *J Cereb Blood Flow Metab* 33(8):1197–1206. doi:10.1038/jcbfm.2013.68
  22. Liu P, Zhao H, Wang R, Wang P, Tao Z, Gao L, Yan F, Liu X, Yu S, Ji X, Luo Y (2015) MicroRNA-424 protects against focal cerebral ischemia and reperfusion injury in mice by suppressing oxidative stress. *Stroke* 46(2):513–519. doi:10.1161/STROKEAHA.114.007482
  23. Longa EZ, Weinstein PR, Carlson S, Cummins R (1989) Reversible middle cerebral artery occlusion without craniectomy in rats. *Stroke* 20(1):84–91
  24. Brait VH, Jackman KA, Walduck AK, Selemidis S, Diep H, Mast AE, Guida E, Broughton BR, Drummond GR, Sobey CG (2010) Mechanisms contributing to cerebral infarct size after stroke: gender, reperfusion, T lymphocytes, and Nox2-derived superoxide. *J Cereb Blood Flow Metab* 30(7):1306–1317. doi:10.1038/jcbfm.2010.14
  25. Yang Y, Shuaib A, Li Q (1998) Quantification of infarct size on focal cerebral ischemia model of rats using a simple and economical method. *J Neurosci Methods* 84(1-2):9–16
  26. Sun L, Jin Y, Dong L, Sumi R, Jahan R, Li Z (2013) The neuroprotective effects of *Coccomyxa gloeobotrydiformis* on the ischemic stroke in a rat model. *Int J Biol Sci* 9(8):811–817. doi:10.7150/ijbs.6734
  27. Jie P, Hong Z, Tian Y, Li Y, Lin L, Zhou L, Du Y, Chen L, Chen L (2015) Activation of transient receptor potential vanilloid 4 induces apoptosis in hippocampus through downregulating PI3K/Akt and upregulating p38 MAPK signaling pathways. *Cell Death Dis* 6: e1775. doi:10.1038/cddis.2015.146
  28. Chen W, Xu B, Xiao A, Liu L, Fang X, Liu R, Turlova E, Barszczyk A, Zhong X, Sun CL, Britto LR, Feng ZP, Sun HS (2015) TRPM7 inhibitor carvacrol protects brain from neonatal hypoxic-ischemic injury. *Mol Brain* 8:11. doi:10.1186/s13041-015-0102-5
  29. Chen J, Simon RP, Nagayama T, Zhu R, Loeffert JE, Watkins SC, Graham SH (2000) Suppression of endogenous bcl-2 expression by antisense treatment exacerbates ischemic neuronal death. *J Cereb Blood Flow Metab* 20(7):1033–1039. doi:10.1097/00004647-200007000-00002
  30. Shimizu S, Nagayama T, Jin KL, Zhu L, Loeffert JE, Watkins SC, Graham SH, Simon RP (2001) bcl-2 Antisense treatment prevents induction of tolerance to focal ischemia in the rat brain. *J Cereb Blood Flow Metab* 21(3):233–243. doi:10.1097/00004647-200103000-00007
  31. Allen CL, Bayraktutan U (2009) Oxidative stress and its role in the pathogenesis of ischaemic stroke. *Int J Stroke* 4(6):461–470. doi:10.1111/j.1747-4949.2009.00387.x
  32. Chen H, Yoshioka H, Kim GS, Jung JE, Okami N, Sakata H, Maier CM, Narasimhan P, Goeders CE, Chan PH (2011) Oxidative stress in ischemic brain damage: mechanisms of cell death and potential molecular targets for neuroprotection. *Antioxid Redox Signal* 14(8):1505–1517. doi:10.1089/ars.2010.3576
  33. Ding Y, Chen M, Wang M, Li Y, Wen A (2015) Posttreatment with 11-keto-beta-boswellic acid ameliorates cerebral ischemia-reperfusion injury: Nrf2/HO-1 pathway as a potential mechanism. *Mol Neurobiol* 52(3):1430–1439. doi:10.1007/s12035-014-8929-9
  34. Arbour N, Vanderluit JL, Le Grand JN, Jahani-Asl A, Ruzhynsky VA, Cheung EC, Kelly MA, MacKenzie AE, Park DS, Opferman JT, Slack RS (2008) Mcl-1 is a key regulator of apoptosis during CNS development and after DNA damage. *J Neurosci* 28(24):6068–6078. doi:10.1523/JNEUROSCI.4940-07.2008
  35. Carroll RG, Hollville E, Martin SJ (2014) Parkin sensitizes toward apoptosis induced by mitochondrial depolarization through promoting degradation of Mcl-1. *Cell Rep* 9(4):1538–1553. doi:10.1016/j.celrep.2014.10.046
  36. Mori M, Burgess DL, Gefrides LA, Foreman PJ, Opferman JT, Korsmeyer SJ, Cavalheiro EA, Naffah-Mazzacoratti MG, Noebels JL (2004) Expression of apoptosis inhibitor protein Mcl1 linked to neuroprotection in CNS neurons. *Cell Death Differ* 11(11):1223–1233. doi:10.1038/sj.cdd.4401483
  37. Huelsemann MF, Patz M, Beckmann L, Brinkmann K, Otto T, Fandrey J, Becker HJ, Theurich S, von Bergwelt-Baildon M, Pallasch CP, Zahedi RP, Kashkar H, Reinhardt HC, Hallek M, Wendtner CM, Frenzel LP (2015) Hypoxia-induced p38 MAPK activation reduces Mcl-1 expression and facilitates sensitivity towards BH3 mimetics in chronic lymphocytic leukemia. *Leukemia* 29(4):981–984. doi:10.1038/leu.2014.320
  38. Ivanovska I, Ball AS, Diaz RL, Magnus JF, Kibukawa M, Schelter JM, Kobayashi SV, Lim L, Burchard J, Jackson AL, Linsley PS, Cleary MA (2008) MicroRNAs in the miR-106b family regulate p21/CDKN1A and promote cell cycle progression. *Mol Cell Biol* 28(7):2167–2174. doi:10.1128/MCB.01977-07
  39. Petrocca F, Visone R, Onelli MR, Shah MH, Nicoloso MS, de Martino I, Iliopoulos D, Pilozzi E, Liu CG, Negrini M, Cavazzini L, Volinia S, Alder H, Ruco LP, Baldassarre G, Croce CM, Vecchione A (2008) E2F1-regulated microRNAs impair TGFbeta-dependent cell-cycle arrest and apoptosis in gastric cancer. *Cancer Cell* 13(3):272–286. doi:10.1016/j.ccr.2008.02.013
  40. Espinosa-Parrilla Y, Munoz X, Bonet C, Garcia N, Vencesla A, Yiannakouris N, Naccarati A, Sieri S, Panico S, Huerta JM, Barricarte A, Menendez V, Sanchez-Cantalejo E, Dorronsoro M, Brennan P, Duarte-Salles T, B As Bueno-de-Mesquita H, Weiderpass E, Lund E, Clavel-Chapelon F, Boutron-Ruault MC, Racine A, Numans ME, Tumino R, Canzian F, Campa D, Sund M, Johansson M, Ohlsson B, Lindkvist B, Overvad K, Tjonneland A, Palli D, Travis RC, Khaw KT, Wareham N, Boeing H, Nesi G, Riboli E, Gonzalez CA, Sala N (2014) Genetic association of gastric cancer with miRNA clusters including the cancer-related genes MIR29, MIR25, MIR93 and MIR106:

- results from the EPIC-EURGAST study. *Int J Cancer* 135(9):2065–2076. doi:[10.1002/ijc.28850](https://doi.org/10.1002/ijc.28850)
41. Brett JO, Renault VM, Rafalski VA, Webb AE, Brunet A (2011) The microRNA cluster miR-106b~25 regulates adult neural stem/progenitor cell proliferation and neuronal differentiation. *Aging (Albany NY)* 3(2):108–124
  42. Conte I, Banfi S, Bovolenta P (2013) Non-coding RNAs in the development of sensory organs and related diseases. *Cell Mol Life Sci* 70(21):4141–4155. doi:[10.1007/s00018-013-1335-z](https://doi.org/10.1007/s00018-013-1335-z)
  43. Montalban E, Mattugini N, Ciarpica R, Provenzano C, Savino M, Scagnoli F, Prosperini G, Carissimi C, Fulci V, Matrone C, Calissano P, Nasi S (2014) MiR-21 is an Ngf-modulated microRNA that supports Ngf signaling and regulates neuronal degeneration in PC12 cells. *Neuromolecular Med* 16(2):415–430. doi:[10.1007/s12017-014-8292-z](https://doi.org/10.1007/s12017-014-8292-z)
  44. McMahon AC, Barnett MW, O’Leary TS, Stoney PN, Collins MO, Papadia S, Choudhary JS, Komiyama NH, Grant SG, Hardingham GE, Wyllie DJ, Kind PC (2012) SynGAP isoforms exert opposing effects on synaptic strength. *Nat Commun* 3:900. doi:[10.1038/ncomms1900](https://doi.org/10.1038/ncomms1900)
  45. Conte I, Merella S, Garcia-Manteiga JM, Migliore C, Lazarevic D, Carrella S, Marco-Ferreres R, Avellino R, Davidson NP, Emmett W, Sanges R, Bockett N, Van Heel D, Meroni G, Bovolenta P, Stupka E, Banfi S (2014) The combination of transcriptomics and informatics identifies pathways targeted by miR-204 during neurogenesis and axon guidance. *Nucleic Acids Res* 42(12):7793–7806. doi:[10.1093/nar/gku498](https://doi.org/10.1093/nar/gku498)
  46. Mourelatos Z, Dostie J, Paushkin S, Sharma A, Charroux B, Abel L, Rappsilber J, Mann M, Dreyfuss G (2002) miRNPs: a novel class of ribonucleoproteins containing numerous microRNAs. *Genes Dev* 16(6):720–728. doi:[10.1101/gad.974702](https://doi.org/10.1101/gad.974702)
  47. Lagos-Quintana M, Rauhut R, Meyer J, Borkhardt A, Tuschl T (2003) New microRNAs from mouse and human. *RNA* 9(2):175–179
  48. Lai EC, Tomancak P, Williams RW, Rubin GM (2003) Computational identification of Drosophila microRNA genes. *Genome Biol* 4(7):R42. doi:[10.1186/gb-2003-4-7-r42](https://doi.org/10.1186/gb-2003-4-7-r42)
  49. Poliseno L, Salmena L, Riccardi L, Fornari A, Song MS, Hobbs RM, Sportoletti P, Varmeh S, Egia A, Fedele G, Rameh L, Loda M, Pandolfi PP (2010) Identification of the miR-106b~25 microRNA cluster as a proto-oncogenic PTEN-targeting intron that cooperates with its host gene MCM7 in transformation. *Sci Signal* 3(117):ra29. doi:[10.1126/scisignal.2000594](https://doi.org/10.1126/scisignal.2000594)
  50. Zhao ZN, Bai JX, Zhou Q, Yan B, Qin WW, Jia LT, Meng YL, Jin BQ, Yao LB, Wang T, Yang AG (2012) TSA suppresses miR-106b-93-25 cluster expression through downregulation of MYC and inhibits proliferation and induces apoptosis in human EMC. *PLoS One* 7(9):e45133. doi:[10.1371/journal.pone.0045133](https://doi.org/10.1371/journal.pone.0045133)
  51. Bruemmer D, Yin F, Liu J, Kiyono T, Fleck E, Van Herle AJ, Law RE (2003) Expression of minichromosome maintenance proteins in vascular smooth muscle cells is ERK/MAPK dependent. *Exp Cell Res* 290(1):28–37
  52. Hutchison ER, Kawamoto EM, Taub DD, Lal A, Abdelmohsen K, Zhang Y, Wood WH 3rd, Lehmann E, Camandola S, Becker KG, Gorospe M, Mattson MP (2013) Evidence for miR-181 involvement in neuroinflammatory responses of astrocytes. *Glia* 61(7):1018–1028. doi:[10.1002/glia.22483](https://doi.org/10.1002/glia.22483)
  53. Ouyang YB, Lu Y, Yue S, Xu LJ, Xiong XX, White RE, Sun X, Giffard RG (2012) miR-181 regulates GRP78 and influences outcome from cerebral ischemia in vitro and in vivo. *Neurobiol Dis* 45(1):555–563. doi:[10.1016/j.nbd.2011.09.012](https://doi.org/10.1016/j.nbd.2011.09.012)
  54. Dharap A, Bowen K, Place R, Li LC, Vemuganti R (2009) Transient focal ischemia induces extensive temporal changes in rat cerebral microRNAome. *J Cereb Blood Flow Metab* 29(4):675–687. doi:[10.1038/jcbfm.2008.157](https://doi.org/10.1038/jcbfm.2008.157)
  55. Zhang C, Teng F, Tu J, Zhang D (2014) Ultrasound-enhanced protective effect of tetramethylpyrazine against cerebral ischemia/reperfusion injury. *PLoS One* 9(11):e113673. doi:[10.1371/journal.pone.0113673](https://doi.org/10.1371/journal.pone.0113673)